Molecular and Cellular Neuroscience 128 (2024) 103914

Contents lists available at ScienceDirect

Molecular and Cellular Neuroscience

journal homepage: www.elsevier.com/locate/ymcne

The exocyst subunit Sec15 is critical for proper synaptic development and function at the *Drosophila* NMJ

Chris J. Kang [a,1], Luis E. Guzmán-Clavel [a,1], Katherine Lei [a], Martin Koo [a], Steven To [a], John P. Roche [a,b,*]

[a] Neuroscience Program, Amherst College, Amherst, MA 01002, United States of America
[b] Department of Biology, Amherst College, Amherst, MA 01002, United States of America

ARTICLE INFO

Keywords:
Sec15
Recycling endosome
Rab11
Exocyst
Extracellular vesicles
Synaptic transmission

ABSTRACT

The exocyst protein complex is important for targeted vesicle fusion in a variety of cell types, however, its function in neurons is still not entirely known. We found that presynaptic knockdown (KD) of the exocyst component *sec15* by transgenic RNAi expression caused a number of unexpected morphological and physiological defects in the synapse. These include the development of active zones (AZ) devoid of essential presynaptic proteins, an increase in the branching of the presynaptic arbor, the appearance of satellite boutons, and a decrease in the amplitude of stimulated postsynaptic currents as well as a decrease in the frequency of spontaneous synaptic vesicle release. We also found the release of extracellular vesicles from the presynaptic neuron was greatly diminished in the Sec15 KDs. These effects were mimicked by presynaptic knockdown of Rab11, a protein known to interact with the exocyst. *sec15 RNAi* expression caused an increase in phosphorylated Mothers against decapentaplegic (pMad) in the presynaptic terminal, an indication of enhanced bone morphogenic protein (BMP) signaling. Some morphological phenotypes caused by Sec15 knockdown were reduced by attenuation of BMP signaling through knockdown of *wishful thinking (Wit)*, while other phenotypes were unaffected. Individual knockdown of multiple proteins of the exocyst complex also displayed a morphological phenotype similar to Sec15 KD. We conclude that Sec15, functioning as part of the exocyst complex, is critically important for proper formation and function of neuronal synapses. We propose a model in which Sec15 is involved in the trafficking of vesicles from the recycling endosome to the cell membrane as well as possibly trafficking extracellular vesicles for presynaptic release and these processes are necessary for the correct structure and function of the synapse.

1. Introduction

Axon terminals are highly specialized cellular regions where targeted vesicle fusion is vital for a variety of critical synaptic functions, including directional growth of the axon, formation of synaptic sites, and synaptic signaling. Determining the mechanisms that control the correct trafficking and fusion of a diverse population of vesicles remains critical for understanding the development, maintenance, and plasticity of the synapse as well as how these mechanisms may be altered in certain pathologies.

Sec15 is a protein originally identified as critical for vesicle exocytosis in yeast (Novick, 2014). Further characterization revealed it to be a member of a large protein complex called the exocyst that contains the proteins Sec3, Sec5, Sec6, Sec8, Sec10, Sec15, Exo70, and Exo84 (TerBush et al., 1996). Whereas the exocyst is universally required for exocytosis in yeast, it is not essential for general vesicle fusion in multicellular organisms where its role is more variable. In neurons, the function of the exocyst is of special interest as there are many different types of exocytosis that occur, each having unique requirements in their spatial and temporal release mechanisms. Previous studies have found that the exocyst is required for neuronal elongation (Vega and Hsu, 2001; Murthy et al., 2003), neuronal target specificity (Mehta et al., 2005), localization of adhesion molecules (Mehta et al., 2005), and possibly synapse localization (Hazuka et al., 1999). However, in all but one case studied to date there was no involvement of the exocyst in synaptic transmission (Andrews et al., 2002; Murthy et al., 2003; Liebl

* Corresponding author at: Program in Neuroscience, Science Center, 25 East Dr., Amherst College, Amherst, MA 01002, United States of America.
E-mail address: jroche@amherst.edu (J.P. Roche).
[1] These two authors contributed equally to this work.

https://doi.org/10.1016/j.mcn.2023.103914
Received 25 August 2023; Received in revised form 4 December 2023; Accepted 5 December 2023
Available online 11 December 2023

et al., 2005; Mehta et al., 2005; Dupraz et al., 2009). The lone exception was a study looking at the exocyst protein Exo70, a study that indicated that loss of this protein did cause limited synaptic transmission defects (Koon et al., 2018).

The exocyst is thought to derive some of its specificity from its interaction with specific vesicle proteins. In yeast, the exocyst subunit Sec15 binds to the Rab homolog Sec4 (Salminen and Novick, 1989; Guo et al., 1999; Boyd, 2004). Rabs are small GTPase proteins that attach to the surface of vesicles to aid in their proper intracellular trafficking (Cai et al., 2007). Sec4 is present on secretory vesicles and this interaction likely connects the vesicle to the exocyst complex (Guo et al., 1999). In multicellular organisms, Sec15 can bind to Rab11, a rab that associates with vesicles emanating from the recycling endosome (Zhang et al., 2004; Wu et al., 2005) as well as Rab3, a rab that associates with synaptic vesicles (Wu et al., 2005). A Rab11/Sec15 association has been shown to be critical for exocytosis of vesicles that transport recycled proteins to the cell surface in HeLa cells and epithelial cells (Langevin et al., 2005; Takahashi et al., 2012).

Here we have isolated *sec15* in a screen for genes that can alter the localization of presynaptic AZ proteins. We found that reduction of Sec15 led to defects of both the structure and function of the synapse. Tissue specific loss of Sec15 in the presynaptic motor neuron causes a decrease in the number of AZs containing the essential presynaptic protein Bruchpilot (BRP). In addition, knockdown of Sec15 causes defects in evoked and spontaneous postsynaptic currents and inappropriate budding/branching of the synaptic terminal. Consistent with a Sec15 interaction with Rab11, a presynaptic knockdown of Rab11 mimicked the phenotype seen in the *UAS-sec15* RNAi lines. We also found that knockdown of Sec15 disrupted the release of extracellular vesicles from the presynaptic neuron, a process previously known to be dependent on Rab11 (Korkut et al., 2013). Additionally, Sec15 KD also enhanced BMP signaling, suggesting phenotypic effects could be a result of activation of this signaling pathway. We found, however, that blocking the enhancement of BMP signaling by knockdown of the BMP receptor Wit did not eliminate the morphologic or synaptic transmission phenotypes seen in Sec15 RNAi knockdowns, suggesting the phenotypes seen after Sec15 knockdown were the result of a combination of direct and indirect effects. In addition, we found that RNAi knockdown of sec*3,* sec*5,* sec*6,* sec*8, sec10* and *exo84* also led to morphological defects similar to *sec15*, suggesting involvement of the entire exocyst complex. Taken together, our data indicate that Sec15, and likely the entire exocyst, plays an important role in regulating the growth and insuring proper function of neuronal synapses.

2. Materials and methods

2.1. Fly stocks

Flies were maintained at 25 °C on standard fly food. Wild-type control animals were Canton S (CS) outcrossed to elav-Gal4 (Yao and White, 1994) and *UAS-DCR2* (Dietzl et al., 2007). The following mutant strains were obtained from the Bloomington Stock Center: wit^{A12}, wit^{B11} (Marqués et al., 2002), and $endoA^{Ey02730}$ (Bellen, 2004). $rab3^{rup}$ (Graf et al., 2009) was also used in this study. The following *UAS-RNAi* lines were obtained from the Bloomington Stock Center: *sec15* TRiP.JF02649 (27499), sec*5* TRiP.GLC01676 (50556), sec*6* TRiP.JF02623 (27314), *exo84*TRiP.JF03139 (28712), *rab11* TRiP.JF02812 (27730), *wishful thinking* TRiP.JF01969 (25949), *sec10* TRiP.JF02633 (27483), saxophone TRiP.JF03431 (36131). The following *UAS-RNAi* lines were obtained from the Vienna *Drosophila* Resource Center (VDRC): *rab3* KK 108633 (100787), *sec15* KK 101708 (105126), *sec15* GD 12109 (35161), sec*3* GD 10687 (35806) sec*8* KK 101531 (105653). RNAi resistant *sec15* was synthesized by VectorBuilder (Chicago, IL). The codon optimized sequence was cloned into the pUAStB vector and injected into flies using phiC31 integrase at the attP2 locus.

2.2. Electrophysiology

Experiments were performed on wandering third instar *Drosophila* larvae reared at 25C. Larvae were dissected in ice-cold low calcium HL-3 media and the segmental nerves were cut. The HL-3 media was then replaced with room temperature modified HL-3 with the following composition (in mM): 70 NaCl, 5 KCl, 10 $MgCl_2$, 10 NaH_2CO_3, 5 Trehalose, 115 Sucrose, 0.7 $CaCl_2$. Electrodes filled with 3 M KCl with resistances between 10 and 20 MΩ were used to impale muscle 6 of either segment A3 or A4 of the filleted larvae. Using an Axon Instruments Axoclamp 2B amplifier, the muscle was then voltage clamped with a holding potential of −70 mV and spontaneous currents were recorded. The segmental nerve was drawn in to a suction electrode and a 3 ms stimulus was given at a level sufficient to fully activate synaptic currents at the NMJ. The resulting evoked synaptic currents were acquired using an ITC-18 (HEKA Electronics) digitizer and recorded using Patchmaster (HEKA Electronics) software. Cells requiring 1 nA or more holding current were discarded. Spontaneous events were recorded for 1 min and the average amplitude and frequency of the spontaneous events was quantified using Mini Analysis Software (Synaptosoft Inc.). For stimulated EJCs, $AgCl_2$ wire in a glass suction electrode was used to stimulate the cut end of the segmental nerve for 1 ms at 1.5× the threshold voltage. A Master 8 (A.M.P.I.) stimulator and Isoflex stimulation isolation unit (A.M.P.I.) were used to control the duration and amplitude of the stimulation. The elicited currents from 10 successive stimulations at 0.5 hz were averaged offline using custom programs written by Josef Trapani (Amherst College) in Igor Pro software (WaveMetrics Inc.). For stimulus trains, the nerve was stimulated with 5 suprathreshold pulses at 20 Hz with 5 s rest intervals between trains. 5 consecutive trains were averaged and the amplitudes of the 1st and 5th pulse were used to calculate the facilitation ratio.

2.3. Immunohistochemistry

Third-instar larvae were dissected in PBS and fixed in 4 % paraformaldehyde fixative for 20 min. Larvae were washed with PBS containing 0.1 % Triton X-100 (PBT) and blocked in 5 % NGS in PBT for 30 min, followed by overnight incubation in primary antibodies in 5 % NGS in PBT, three washes in PBT, incubation in secondary antibodies in 5 % NGS in PBT for 45 min, three final washes in PBT, and equilibration in 70 % glycerol in PBS. Samples were mounted in VectaShield (Vector, Burlingame, CA). The following primary antibodies were used: mouse α-BRP, 1:250 (Developmental Studies Hybridoma Bank); rabbit α-DGluRIII, 1:2500 (Marrus, 2004); rabbit α-phosphorylated MAD, 1:500 (gift of P. ten Dijke, Leiden University, Leiden, The Netherlands (Persson et al., 1998), mouse α-neuroglian 1:200 (Developmental Studies Hybridoma Bank), mouse α-sec15 (gift of Hugo Bellen),rabbit α-GFP, 1:1000 (NOVUS Biologicals), mouse α-β-tubulin (1:1000; E7, Developmental Studies Hybridoma Bank). Cy3-conjugated goat antibodies against mouse, Alexa −488-conjugated goat antibodies against rabbit, and Cy5-conjugated goat α-HRP were used at 1:1000 and were obtained from Jackson ImmunoResearch. Antibodies obtained from the Developmental Studies Hybridoma Bank were developed under the auspices of the National Institute of Child Health and Human Development and maintained by the Department of Biological Sciences of the University of Iowa, Iowa City, IA.

2.4. Imaging and analysis

Samples were imaged using a Nikon (Tokyo, Japan) C2 confocal microscope or a Zeiss laser Scanning Microscope 980(Carl Zeiss Microscopy) with an Airyscan 2 (GaAsP-PMT) detector.

All genotypes for an individual experiment were imaged at the same gain and set such that signals from the brightest genotype for a given experiment were not saturating. Only type 1b NMJs on muscle 4 were analyzed.

Confocal images were analyzed using MetaMorph (Molecular Devices, Sunnyvale, CA) and FIJI (Schindelin et al., 2012) software. Airyscan images were processed using the Airyscan processing, utilizing in all cases Zen Blue Software (Carl Zeiss Microscopy).

Statistical analysis was performed using 1-way ANOVA for comparison of multiple samples within an experimental group with a Tukey's post -hoc test for comparison of individual values. For comparisons in experiments with only two groups, the Student's *t*-test was utilized. All statistical data is included in a supplemental table (Supplemental Table 1). All bar graphs and measurements are shown as mean ± SEM. To determine the percentage of GluR clusters apposed by BRP, BRP and DGluRIII puncta were manually counted, and DGluRIII clusters that were not opposite to a detectable BRP punctum were counted as unapposed DGluRIII clusters. MetaMorph and/or FIJI software was used for the quantification of average intensity. FIJI was used for BRP puncta area in Airyscan images. For measurements of antibody intensity per NMJ area, the area of the NMJ was first defined by HRP signal. The average intensity of antibody signal within each defined NMJ was then calculated, and the average muscle background intensity was subtracted. Satellite boutons were quantified by counting any single bouton emanating from the main chain. Two or more consecutive boutons emanating from the main chain were counted as a branch. For the extracellular vesicle analysis we created an ROI that outlines the HRP-marked neuronal membrane in Image-J. We then enlarged the ROI by 1.5 μm, termed hereafter as ROI + 1.5. We analyzed the integrated density (ID) and area of both ROIs. We quantified extracellular vesicle release as: ID(ROI + 1.5) − ID(ROI). Accounting for area: [ID(ROI + 1.5) − ID(ROI)] / [area(ROI + 1.5) − area(ROI)].

2.5. Western blots

Third-instar larval brains were homogenized in 1× Laemmli sample buffer (10 μL 4× Biorad Laemmli sample buffer (formulation: 65.8 mM Tris-HCl, pH 6.8, 2.1 % SDS, 26.3 % (*w/v*) glycerol, 0.01 % bromophenol blue), 4.5 μL 2-mercaptoethanol, and 25.5 μL Biology Grade Water), and samples were run on 10 % Mini-PROTEAN Protein Gels at 200 V for 35 min at RT. Gels were transferred to nitrocellulose membranes using transfer buffer at 100 V for 60 min at 4 °C. The primary antibodies utilized were guinea pig α-sec15 (1:1000) (gift of Hugo Bellen) and mouse α-β-tubulin (1:1000; E7, Developmental Studies Hybridoma Bank). For secondary antibodies, 680RD goat anti-mouse (1:20,000) and 800CW donkey anti-guinea pig (1:20,000) (LI-COR Biosciences) were utilized. The mean intensity of each beta-tubulin band (~55 kDa) was quantified as our loading control, as well as each band of sec15 (~95 kDa) through the LI-COR CLx Odyssey Infrared Imaging System. The mean intensity of each sec15 band was then normalized to the intensity of the beta-tubulin band of its respective lane. Finally, the results were then expressed as a percentage of the maximal response.

2.6. Experimental design and statistical analysis

All statistical analysis was performed using Prism software (GraphPad Software, San Diego, CA). Data were reported as mean ± SEM. For comparisons of two samples the unpaired Student's *t*-test was used to determine statistical significance. For experiments with 3 or more groups we used 1-way ANOVA with Tukey's post-hoc test to determine significance of specific groups. In all cases the significance was reported as either non-significant (ns) or significant at <0.05, <0.01, or <0.001 level. In all figures * denotes significant difference at the $p < 0.05$, ** $p < 0.01$, or*** $p < 0.001$ level. A supplemental table has been included showing the statistics for each experiment including the n and p values for each comparison. (Supp. Table 1).

3. Results

3.1. Sec15 RNAi enhances Rab3 mutant phenotype

The *Drosophila* larval NMJ is composed of a motor neuron that contacts a muscle during development. As development proceeds the muscle enlarges and, in order to maintain the ability to excite the growing muscle, the presynaptic neuron contacting the muscle enlarges as well. The expansion of the NMJ during development occurs by the sequential addition of boutons, forming a string of boutons with an occasional branchpoint (Zito et al., 1999). Within each bouton are multiple AZs, sites of synaptic vesicle release, where presynaptic proteins required for efficient vesicle release aggregate opposite postsynaptic glutamate receptors clustered in the muscle membrane.

Previous studies have identified a synaptic vesicle protein, called Rab3, as essential in the correct expression of some presynaptic proteins in the presynaptic active zone (Graf et al., 2009). In wild type NMJs, the presynaptic protein BRP is localized at nearly all AZs. However in the *rab3* mutant as well as *rab3* RNAi knockdowns, BRP aggregates in enlarged clusters at only a fraction of AZs, leaving the majority devoid of essential presynaptic proteins (Graf et al., 2009, 2012). The mechanism by which Rab3 aids in localizing synaptic proteins is currently unknown. Towards the goal of understanding Rab3's function, we sought to identify genes that may aid Rab3 in the development of AZs. To do this we performed a forward genetic screen in a *rab3* RNAi knockdown background previously shown to cause a synaptic apposition phenotype characterized by the loss of BRP puncta in a subset of active zones (Graf et al., 2009, 2012). The use of the *rab3* RNAi line enhanced the likelihood of identifying genes genetically interacting with *rab3* as the *rab3* RNAi knockdown acted as a hypomorph compared to the *rab3* null mutant. Thus, we could identify genes that may act in the same molecular pathway by identifying genes capable of enhancing the apposition phenotype of the Rab3 RNAi hypomorph to match the Rab3 apposition phenotype seen in the Rab3 null mutant. We screened an RNAi library to identify genes that could enhance the *rab3* RNAi knockdown phenotype. Using the mislocalization of presynaptic BRP produced by expression of a *UAS-RNAi* transgene against *rab3* as a sensitized background, we screened over 1000 genes for the ability to modify this phenotype.

Individual fly lines containing a selection of *UAS-RNAi* transgenes were crossed to a fly line containing *UAS-rab3 RNAi, UAS-dicer2 (DCR2)* and the neuronal *elav-Gal4* driver to produce progeny wherein both *rab3* and a second gene are knocked down. With this method, we isolated several candidate genes that enhanced the severity of the apposition phenotype produced by *UAS-Rab3 RNAi* expression. One such gene isolated was a gene encoding a protein called Sec15. Driving *UAS-sec15 RNAi* in neurons concurrently with *UAS-rab3 RNAi* caused a significant decrease in the percentage of glutamate receptor clusters apposed by BRP-positive presynaptic AZs as compared to the expression of *UAS-rab3 RNAi* alone (Fig. 1A, C). As RNAi can have off target effects (Echeverri et al., 2006; Sigoillot and King, 2011), we tested other RNAi lines that target other regions of the *sec15* gene. We found two additional RNAi lines that also caused a similar decrease in the percentage of glutamate receptor clusters apposed to BRP, suggesting the phenotype resulted specifically from the knockdown of Sec15.

sec15 codes for a protein that exists as part of a multi-protein exocyst complex that aids in targeted vesicle exocytosis (Hsu et al., 2004; Wu and Guo, 2015). Prior in vitro biochemical evidence suggested that Sec15 can bind to Rab3 (Wu et al., 2005). This finding in conjunction with our observed enhancement of the *rab3* AZ phenotype by concurrent knockdown of Sec15 led us to hypothesize that Sec15 may act as a Rab3 effector to control AZ development. This hypothesis predicts that individual knockdown of Sec15 should result in an apposition phenotype

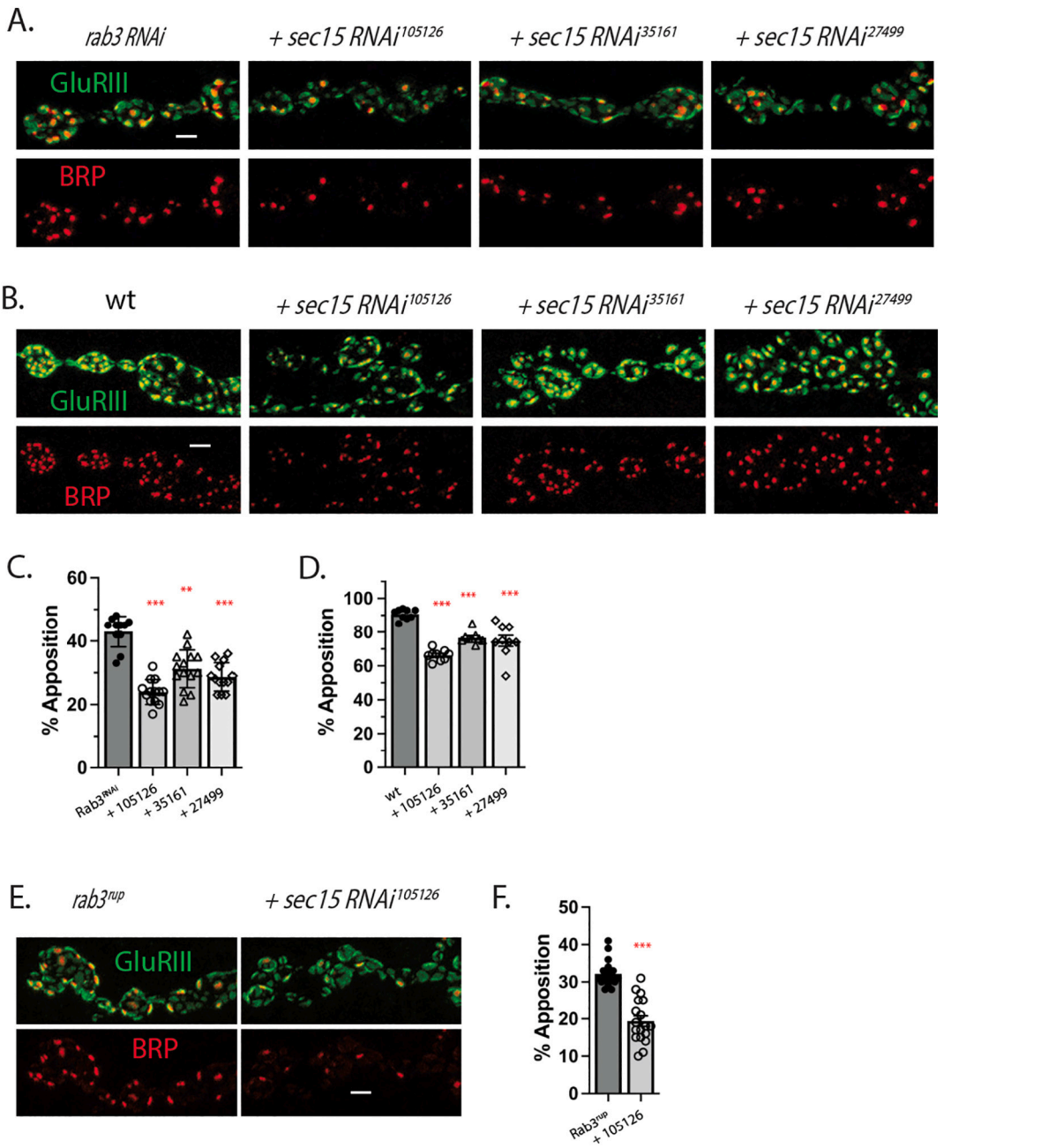

Fig. 1. Sec15 enhances the *rab3* active zone apposition phenotype. **A)** Confocal images of representative type 1b synaptic boutons of muscle 4 NMJs from larvae expressing a *rab3 RNAi* transgene alone (*UAS-DCR2, elav-Gal4/+; UAS-Rab3 RNAi/+*) or in combination with one of three different *sec15* RNAi transgenes: *+sec15 RNAi*^{105126} (*UAS-DCR2, elav-Gal4/UAS-sec15 RNAi*^{105126}; *UAS-Rab3 RNAi/+*), *+sec15 RNAi*^{35161} (*UAS-DCR2, elav-Gal4/+; UAS-Rab3 RNAi/UAS-sec15 RNAi*^{35161}), and *+sec15 RNAi*^{27499} (*UAS-DCR2, elav-Gal4/+; UAS-Rab3 RNAi/UAS-sec15 RNAi*^{27499}). The upper images are labeled with α-BRP (red) and α-GluRIII (green), while the lower images show the α-BRP (red) signal only. Scale bar is equal to 2 μm **B)** Confocal images of the muscle 4 NMJs labeled with α-BRP (red), and α-GluRIII (green) from wild type larvae (*elav-Gal4, UAS-DCR2/+*) or larvae expressing one of three *UAS-sec15 RNAi* transgenes: *sec15 RNAi*^{105126} (*elav-Gal4, UAS-DCR2/UAS-sec15 RNAi*^{105126}), *sec15 RNAi*^{35161} (*elav-Gal4, UAS-DCR2/+; UAS-sec15 RNAi*^{35161}*/+*), and *sec15 RNAi*^{27499} (*elav-Gal4, UAS-DCR2/+; UAS-sec15 RNAi*^{27499}*/+*). Scale bar is equal to 2 μm **C)** Bar graphs illustrating % of GluRIII clusters apposed by a BRP punctum from the genotypes listed in (A). ***denotes significant difference at the $p < 0.001$ level using 1-way ANOVA with Tukey's post-hoc test. **D)** Bar graph of %GluRIII clusters apposed by a BRP punctum from the genotypes listed in (B). **, *** denotes significant difference at the $p < 0.01$ or $p < 0.001$ level respectively using 1-way ANOVA with Tukey's post-hoc test. **E)** Confocal images of synaptic boutons of muscle 4 NMJs labeled with α-BRP (red), and α-GluRIII (green) from the rab3 null mutant *rab3*^{rup} (*rab3*^{rup}*/rab3*^{rup}) or in combination with a *sec15* RNAi^{105126} transgene, *+sec15 RNAi*^{105126} (*UAS-DCR2, elav-Gal4/UAS-sec15 RNAi*^{105126}; *rab3*^{rup}*/rab3*^{rup}). Scale bar is equal to 2 μm **F)** Bar graph illustrating % GluRIII receptor clusters apposed by BRP punctum for the genotypes listed in (E).

that is similar to Rab3 knockdown. Driving the *UAS-sec15 RNAi* transgene in a wild-type background resulted in an apposition phenotype where approximately 20–30 % of postsynaptic GluR clusters were not apposed to a BRP punctum (Fig. 1B, D), indicating that loss of Sec15 plays a role in BRP localization by itself and not just in conjunction with the loss of Rab3. This effect was not Gal4 driver specific, as similar results were obtained using the elav (Fig. 1B, D) and vGlut (OK371) drivers (Fig. S1). The sec15 phenotype seen was not similar to the Rab3 phenotype as, although there was mis-apposition, the remaining BRP puncta were not enlarged as is seen on Rab3 KDS and mutants (Fig. 1A,

B), suggesting Rab3 and Sec15 act via independent mechanisms.

To further investigate whether Sec15 acts in the same mechanistic pathway as Rab3 or in a separate pathway, we next asked whether the effects of *sec15* knockdown could be occluded by complete loss of Rab3. The concurrent *sec15*, *rab3* RNAi knockdown results in an AZ phenotype similar in magnitude to the $rab3^{rup}$ null mutant. As stated previously, knockdown of Rab3 by *UAS-rab3 RNAi* results in a weaker hypomorphic phenotype as compared to the null $rab3^{rup}$ mutant (Graf et al., 2012). We hypothesized that if Rab3 and Sec15 act together as part of the same molecular mechanism or pathway, knockdown of *sec15* in the null $rab3^{rup}$ mutant should not enhance the $rab3^{rup}$ mutant phenotype. Conversely, if the two proteins act through different mechanisms or pathways, we would expect an additive effect. Thus, to differentiate between these two options, we drove a *UAS-sec15 RNAi* transgene in the $rab3^{rup}$ mutant background. When we compared the Sec15 knockdown in a $rab3^{rup}$ background to the *rab3* null mutant we found that the percentage of GluR clusters apposed to BRP decreased (Fig. 1E, F), suggesting Rab3 and Sec15 are acting independently to reduce synaptic apposition.

3.2. Sec15 RNAi causes multiple synaptic morphological defects

Our work indicates that Sec15 knockdown results in defective AZ development. We next asked whether loss of Sec15 causes additional defects in NMJ development. Prior studies of exocyst subunits in *Drosophila* have indicated that sec15 null mutants were lethal and animals did not live past the second instar stage (Mehta et al., 2005). Knowing this, we decided to analyze the gross NMJ morphology in larvae expressing the three different *UAS-sec15 RNAi* transgenes by staining with an anti-HRP antibody. Individual expression of all three *UAS-sec15 RNAi* transgenes resulted in increased branching of the presynaptic neuronal arbor (Fig. 2A, B) and an increase in the appearance small boutons emanating from a larger bouton of a main branch in all but one sec15 RNAi construct (Fig. 2A, C). These small boutons emanating from the main branch are frequently termed satellite boutons (Torroja et al., 1999; Dickman et al., 2006; O'Connor-Giles and Ganetzky, 2008). Western blots confirmed that Sec15 was indeed knocked down to about 25 % of control levels after the expression of the *uas-sec15 RNAi* constructs (Fig. 2D, E). Thus, loss of Sec15 results in altered growth of the axon terminal in addition to defective aggregation of BRP at presynaptic AZs.

The fact that three separate RNAi targeted to different regions of *sec15* all produced similar phenotype was good evidence that we were specifically targeting *sec15*. To further test for specificity we utilized a *UAS-sec15* that was RNAi resistant and expressed it in neurons using the Elav-Gal4 driver to rescue the phenotype observed with KD of *sec15*. We co-expressed this *UAS-sec15* construct with the *sec15* RNAi and found that % apposition, NMJ branching, and the number of satellite boutons/NMJ all returned to wt levels (Fig. 3 A, B, C). These data, together with the phenotypes seen with three different *sec15* RNAi's, indicate we are observing phenotypes that result from the specific knock down of Sec15.

3.3. Sec15 knockdown causes defects in synaptic physiology

Since we observed that Sec15 knockdown causes both morphological defects in NMJ structure as well as more specific AZ defects, we next asked whether loss of Sec15 results in functional defects at the synapse. Prior studies in *Drosophila* using mutant alleles of exocyst component genes have noted the lack of effect on synaptic transmission (Andrews et al., 2002; Murthy et al., 2003; Mehta et al., 2005). These studies, however, were hampered by the lethality of exocyst mutants. The use of RNAi allowed us to more directly address this question in *Drosophila,* as neuron-specific knockdown does not cause lethality. We could thus drive *sec15* RNAi specifically in neurons using the *elav-Gal4* driver and

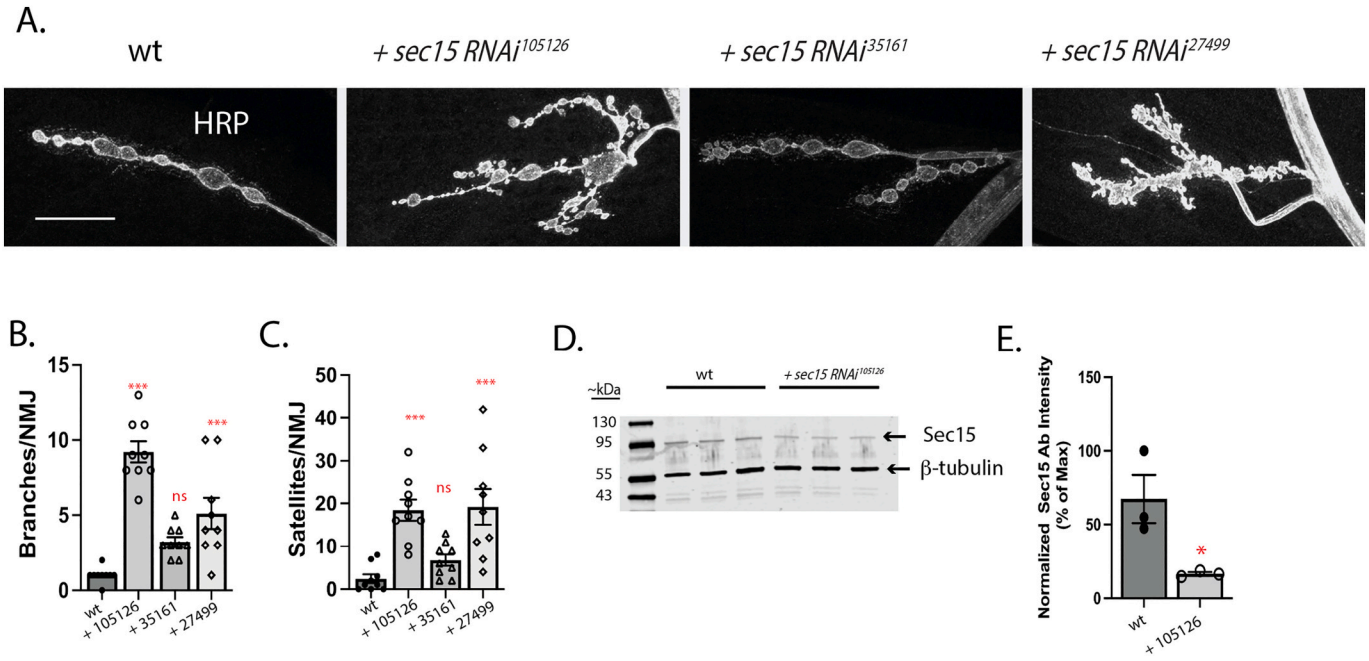

Fig. 2. Sec15 knockdown causes significant morphological phenotypes at the *Drosophila* NMJ. Confocal images of the NMJ of Drosophila 3rd instar larval muscle 4. Preparations are labeled with antibodies to HRP (Blue). **A)** Confocal images of the muscle 4 NMJs labeled with α-HRP (blue) from wild type larvae (*elav-Gal4, UAS-DCR2/+*) or larvae expressing one of three *UAS-sec15 RNAi* transgenes: *sec15* $RNAi^{105126}$ (*elav-Gal4, UAS-DCR2/UAS-sec15* $RNAi^{105126}$), *sec15* $RNAi^{35161}$ (*elav-Gal4, UAS-DCR2/+; UAS-sec15* $RNAi^{35161}$*/+*), and *sec15* $RNAi^{27499}$ (*elav-Gal4, UAS-DCR2/+; UAS-sec15* $RNAi^{27499}$*/+*). Scale bar is equal to 20 μm. **B)** Bar graphs illustrating the average number of branches and **C)** average number of satellite boutons in NMJ from listed genotypes in A. ***denotes significant difference at the $p < 0.001$ level using 1-way ANOVA with Tukey's post-hoc test. **D)** Western blot of wt and Sec15 RNAi larvae stained with anti-sec15 and anti β-tubulin, showing bands at the predicted molecular weights of 88.7 kDa and 49.9 kDa for Sec15 and β-tubulin respectively. **E)** Bar graph showing the quantification of the Sec15 intensity seen in the western blot shown in Fig. 2D. * denotes significant difference at the $p < 0.05$ level using Student's *t*-test. (For interpretation of the references to colour in this figure legend, the reader is referred to the web version of this article.)

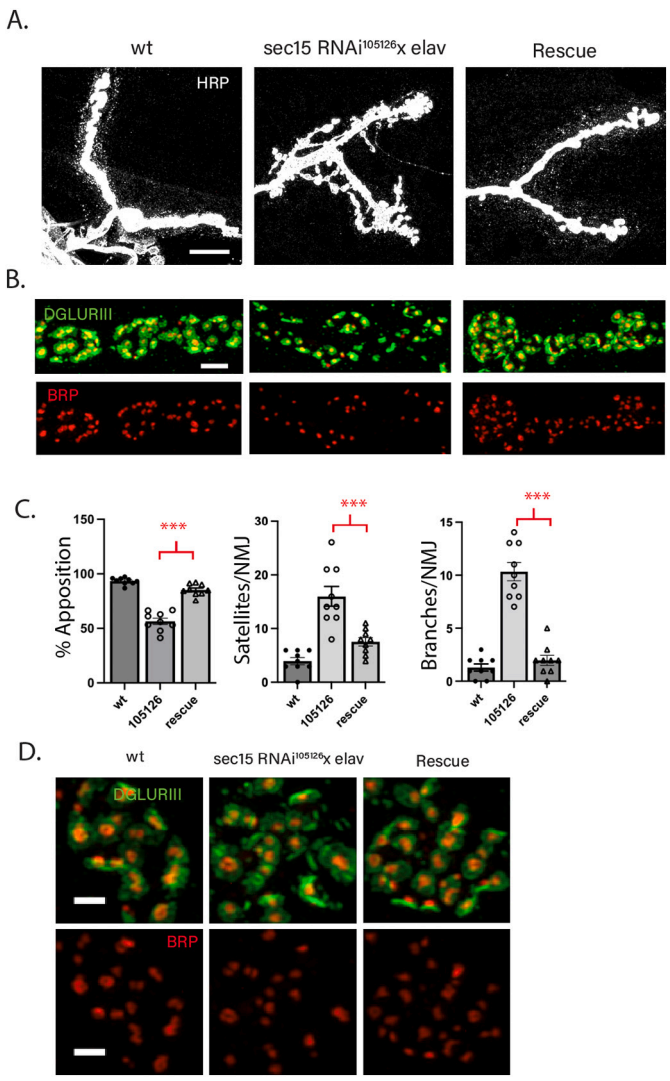

Fig. 3. Expression of RNAi resistant sec15 rescues sec15KD phenotypes. To confirm the specificity of our RNAi construct, we expressed an RNAi resistant UAS- Sec15 in conjunction with sec15 RNAi (rescue). **A)** Representative image of NMJs of wt, sec15 RNAi, and sec15 RNAi + uas-sec15 (rescue). NMJs are stained with HRP (white). Scale bar represents 20 μm. **B)** Enlarged section of NMJs displaying apposition. NMJs are stained for α-GluRIII (Green) and α-Brp (Red). Scale bar represents 2 μm. **C)** Quantification of apposition between DGluRIII and Brp puncta (left), number of satellite boutons/NMJ (middle) and number of branches/NMJ (right). **D)** Representative images of NMJs stained with α-GluRIII (Green) and α-Brp (Red). Scale bar represents 1 μm. For all graphs * denotes significant difference at the * $p < 0.05$, ** $p < 0.01$, *** $p < 0.001$ level using one-way ANOVA with Tukey's post-hoc test.

the resulting flies survive to pupation, allowing us to directly address the effects of the presynaptic loss of Sec15.

To assess NMJ function, we first examined spontaneous synaptic currents in 3rd instar wild-type larvae and larvae expressing the *UAS-sec15 RNAi* transgenes. The amplitude of miniature excitatory junctional currents (mEJCs) from NMJs expressing *sec15* RNAi was unchanged from wild-type (Fig. 4A, D); however, there was a dramatic decrease in mEJC frequency (Fig. 4A, E). We next tested the synaptic response to stimulation of the segmental nerve and found that *sec15* knockdown caused a large decrease in evoked excitatory junctional current (EJC) amplitude (Fig. 4B, F). Since mEJC amplitude was unchanged this resulted from a dramatic decrease in number of synaptic vesicles released per stimulus (quantal content) (Fig. 4G). Decreased quantal content can result from a reduction in the probability of vesicle release at release sites. To determine whether *UAS-sec15 RNAi* expression caused a change in release probability, we tested the response of the synapse to a train of 5 stimuli at 20 Hz and calculated the facilitation ratio, an assay frequently used as a measure of release probability (Graf et al., 2009; Regehr, 2012). The NMJs of two of the three *UAS-sec15* RNAi -expressing larvae displayed a significantly larger facilitation ratio, indicative of a lower initial release probability (Fig. 4C, H). To further test the specificity of the RNAi used as it relates to this specific phenotype, we repeated these experiments with the addition of our RNAi resistant *sec15* construct. We found that the construct completely rescued the decrease in mEJC frequency, while the rescue of the EJC amplitude trended towards wt levels but did not rise to the level of statistical significance (Fig. S2). Thus, in addition to the morphological phenotypes observed following reduction of Sec15, there are significant defects in both spontaneous and stimulated synaptic currents.

3.4. RNAi directed towards other exocyst subunits also causes morphological defects similar to sec15

In yeast, the entire exocyst is required for vesicle secretion (Novick, 2014). An interesting finding in previous work looking at the effects of *sec15* disruption in *Drosophila* retinal neurons was that the entire exocyst complex was not necessary for the actions of Sec15. In this study, the authors found subcomplexes including Sec15, Sec5, and Sec8 but not Sec6 may in certain circumstances mediate exocyst function (Mehta et al., 2005). This result raised the possibility that sub-complexes of the exocyst may be important for mediating some of the effects associated previously with the entire exocyst. To determine a possible contribution of other exocyst subunits, we utilized RNAi transgenes targeted against other exocyst subunits to determine if they could reproduce the morphological phenotypes seen with Sec15 knockdown. We found that indeed several other exocyst subunit RNAi could reproduce the phenotype. Expression of RNAi transgenes against sec*5, sec10* and *exo84* was capable of causing mislocalization of the AZ component BRP, similar to that seen with *UAS-sec15 RNAi* (Fig. 5B). Branching of the NMJ was significantly increased when driving UAS-RNAi transgenes against *sec5,* sec*6, sec10* and *exo84* in the presynaptic neuron (Fig. 5A, C, D). Formation of satellite boutons was significantly enhanced in all exocyst subunits tested with the exception of *exo70*. RNAi transgenes against exocyst subunit *exo70* were in fact unable to reproduce any of the morphological synaptic phenotypes. However, this does not preclude exo70 from acting as part of the complex as some RNAi transgenes are ineffective at reducing their targeted protein. In addition, Exo70 has been implicated in growth of the *Drosophila* NMJ (Koon et al., 2018). Thus, at the neuromuscular junction of *Drosophila*, it is not an exocyst protein subcomplex similar to that seen in the retina and is more likely the entire exocyst complex that is necessary to maintain proper morphology at the synapse.

3.5. RNAi knockdown of rab11 mimics both morphological and physiological effects of sec15 knockdown

The appearance of increased branching and increased satellite boutons following *sec15* knockdown was reminiscent of several mutants in the vesicle endocytic and recycling pathways (Koh et al., 2004; Marie et al., 2004; Dickman et al., 2006; Khodosh et al., 2006; O'Connor-Giles and Ganetzky, 2008; Rodal et al., 2008; Liu et al., 2014). One protein in this pathway is Rab11, a vesicle-associated Rab that is localized to recycling endosomes. The loss of Rab11 results in the growth of satellite boutons (Khodosh et al., 2006), and Rab11 can colocalize with Sec15 (Zhang et al., 2004; Wu et al., 2005) as well as bind Sec15 (Wu et al., 2005). Thus, we hypothesized that Sec15 may control NMJ morphology and physiology via an interaction with Rab11. If this were the case, the effects of a Rab11 knockdown should mimic Sec15 knockdown.

To compare the developmental and functional defects caused by loss of Rab11 and Sec15, we expressed a *UAS-Rab11 RNAi* transgene

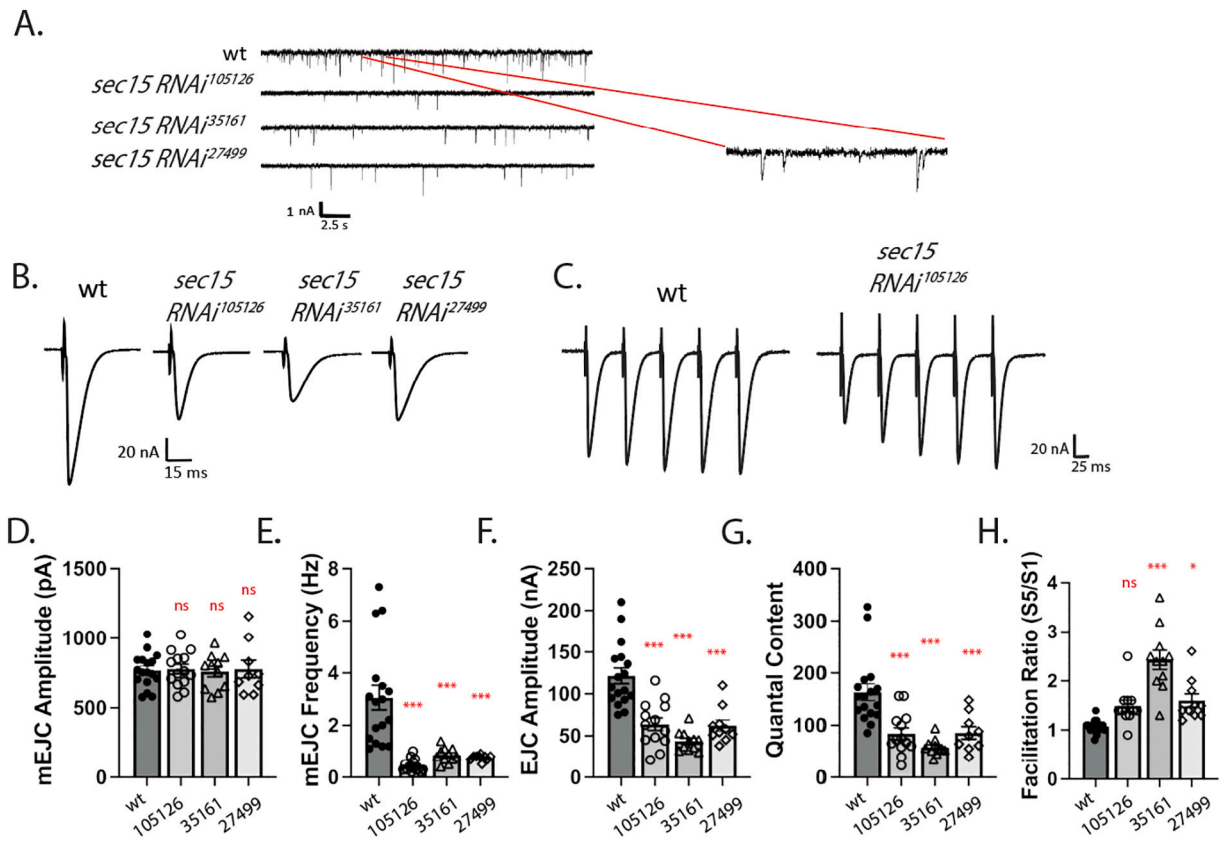

Fig. 4. Sec15 knockdown results in multiple physiological defects at the NMJ. **A)** Two Electrode electrophysiological recordings from muscle 6 of 3rd instar Drosophila larvae voltage clamped to −70 mV. Representative traces displaying spontaneous release events (minis) for wild type (*elav-Gal4, UAS-DCR2/+*), or larvae expressing one of three *UAS-sec15 RNAi* transgenes: *sec15 RNAi*^{105126} (*elav-Gal4, UAS-DCR2/UAS-sec15 RNAi*^{105126}), *sec15 RNAi*^{35161} (*elav-Gal4, UAS-DCR2/+; UAS-sec15 RNAi*^{35161}*/+*), and *sec15 RNAi*^{27499} (*elav-Gal4, UAS-DCR2/+; UAS-sec15 RNAi*^{27499}*/+*). Inset is an enlarged section from the wild type recording demonstrating the kinetics of the miniature events. **B)** Representative recordings of stimulated currents elicited by a single suprathreshold electrical pulse for the genotypes listed in (A). Figures show the average current waveform of 10 consecutive stimulations. **C)** Representative recordings of the current facilitation seen with 5 stimulations at 20 Hz for the genotypes listed in the figure. These recordings were used to calculate the facilitation ratio, the amplitude of the 5th EJC divided by the amplitude of the 1st EJC. **D–H)** Quantitation of the average electrophysiological phenotypes seen for the genotypes listed in (A). **D)** Miniature excitatory junctional current (mEJC) amplitude **E)** mEJC frequency **F)** Average EJC amplitude **G)** Average quantal content (EJC/mEJC) **H)** Average facilitation ratio. * denotes significant difference at the * $p < 0.05$, or *** $p < 0.001$ level using 1-way ANOVA with Tukey's post-hoc test.

neuronally using *elav-Gal4* to specifically knockdown Rab11 presynaptically. We found that knockdown of Rab11 in neurons caused a phenotype nearly indistinguishable from that seen for Sec15 knockdown. Morphologically, *UAS-rab11 RNAi* expression reduced the percentage of GluR clusters apposed to BRP (Fig. 6B, C), and caused a dramatic increase in NMJ branching and satellite bouton formation (Fig. 6A, B, D, E). In addition, presynaptic loss of Rab11 resulted in synaptic physiology deficits nearly identical to loss of Sec15. When compared to controls, knockdown of Rab11 resulted in a large decrease in mEJC frequency (Fig. 6F, I). Furthermore, *UAS-rab11 RNAi* expression resulted in decreased EJC amplitude and quantal content similar to that observed following Sec15 knockdown (Fig. 6G, J, K). There was a slight increase in the size of the mEJCs when comparing Rab11 KDs to controls (Fig. 6H), which was not seen in Sec15 KDs. This minor difference in synaptic function may point to a subset of functions that may be separate between Rab11 and Sec15 or alternatively it could simply be a difference in sensitivity of this particular phenotype to the levels of knockdown in the two different RNAi constructs. However, it remains that nearly all of the numerous morphological and functional phenotypes observed following Sec15 knockdown were mimicked by Rab11 knockdown, suggesting that the two proteins act in a shared mechanism. Knockdown of Rab11 and Sec15 concurrently resulted in lethality prior to the third instar stage.

3.6. Knockdown of Sec15 causes an enhancement of BMP signaling

A key regulator for synapse development at the *Drosophila* NMJ is the bone morphogenic (BMP) signaling pathway. In this pathway, a signal generated in the muscle, Glass bottom boat (Gbb), is released and binds to a receptor complex on the motor neuron (McCabe et al., 2003). The receptor complex is made up of the tyrosine kinase receptors Wishful thinking (Wit), Thick veins (Tkv), and Saxophone (Sax) (Keshishian and Kim, 2004; Collins and DiAntonio, 2007). Subsequent to receptor binding the cytoplasmic protein Mothers against decapentaplegic (Mad) is phosphorylated and transported to the nucleus where it regulates gene expression. Activation of this signaling pathway allows for the proper expansion of the neuronal portion of the synapse during larval development (Keshishian and Kim, 2004). The pathway can be enhanced by blocking the endocytic and recycling pathways (Sweeney and Davis, 2002; O'Connor-Giles and Ganetzky, 2008; Liu et al., 2014) as well as removing inhibitory regulators such as *daughters against decapentaplegic* (*dad*) (Sweeney and Davis, 2002). Activation of the BMP signaling pathway causes altered presynaptic development that is characterized by the appearance of a large number of satellite boutons and increased arborization (O'Connor-Giles et al., 2008; Rodal et al., 2008).

As many of the morphological phenotypes of Sec15 knockdown are also frequently seen as a result of over activation of the BMP signaling pathway, we examined the involvement of the BMP signaling pathway

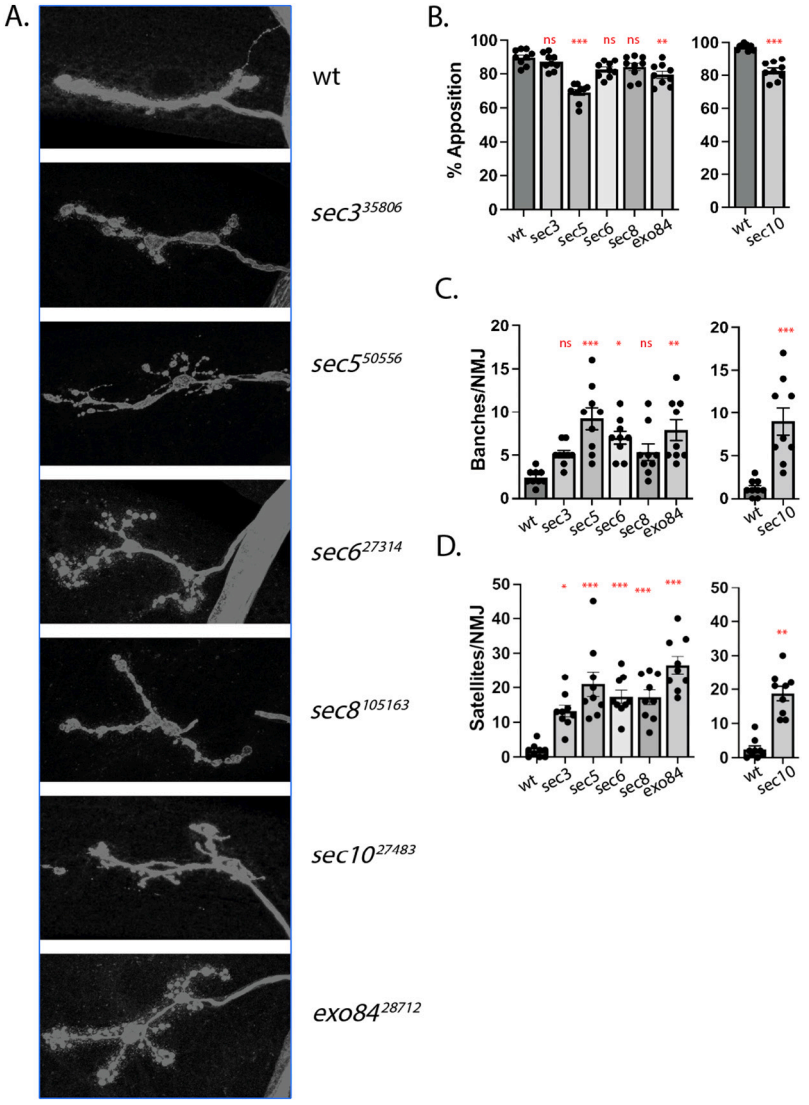

Fig. 5. *UAS-RNAi* for multiple components of the exocyst complex also cause morphological phenotypes similar to *UAS-sec15 RNAi*. **A)** Confocal images of the NMJ of *Drosophila* 3rd instar larval muscle 4. Preparations are labeled with antibodies to HRP (blue), BRP (red), and GluRIII (green). Shown are representative NMJs from (left to right) larvae containing a *UAS-RNAi* directed towards various exocyst subunits including sec*3* (*elav-Gal4, UAS-DCR2/+; UAS-sec3 RNAi* (35806)/+), sec*5* (*elav-Gal4, UAS-DCR2/+; UAS-sec5 RNAi* (50556)/+), sec6 (*elav-Gal4, UAS-DCR2/+; UAS-sec6 RNAi* (27314)/+), sec*8* (*elav-Gal4, UAS-DCR2/+; UAS-sec8 RNAi* (105163)/+), *UAS-sec10* (*elav-Gal4, UAS-DCR2/+; UAS-sec10 RNAi* (27483)/+) and exo84 (*elav-Gal4, UAS-DCR2/+; UAS-exo84 RNAi* (28712)/+). Scale bar is equal to 20 μm. **B–D)** Bar graphs illustrating average morphology of control larvae (*elav-Gal4, UAS-DCR2/+*) and exocyst subunit *RNAi* listed in A, including **B)** percentage of glutamate receptor clusters apposed by BRP clusters **C)** average number of branches per NMJ and **D)** average number of satellite boutons/NMJ. Error Bars represent SEM. * denotes significant difference at the $p < 0.05$, ** $p < 0.01$, or *** $p < 0.001$ level using 1-way ANOVA with Tukey's post-hoc test. A Student's *t*-test was used for 27,483 as that experiment was done separately.

by determining the levels of phosphorylated Mad (pMad) in the NMJ. Mad is phosphorylated by the activated BMP receptor complex and as a result, the amount of pMad increases in situations where the BMP pathway is activated. This effect is considered to be a crucial test for determining the involvement of the BMP pathway (O'Connor-Giles et al., 2008). We found that neuronal expression of a *UAS-sec15 RNAi* transgene in the neuron did indeed cause a marked increase in the pMad levels at the NMJ (Fig. 7A, C). We also wanted to determine if this increase was acting via the BMP signaling pathway. To do this we expressed, concurrently with *sec15* RNAi, a second RNAi designed to knockdown the Wit receptor. Interestingly, knockdown of the presynaptic BMP receptor Wit completely blocked the *UAS-sec15 RNAi*-induced increase in pMad levels (Fig. 7A, C) indicating the sec15 induced enhancement of pMad was indeed mediated via enhanced BMP signaling and also highlighting the effectiveness of the *UAS-wit RNAi* transgene at eliminating BMP signaling.

The enhancement of pMad protein levels was relatively modest compared to that observed in previous studies with other BMP activators (O'Connor-Giles et al., 2008). In order to gauge the level of pMad enhancement caused by Sec15 knockdown, we also tested pMad levels in an *endophilinA* mutant previously shown to display robust pMad enhancement (O'Connor-Giles et al., 2008). In our hands, *endophilinA* mutants caused an increase in pMad similar to levels seen in our Sec15 knockdown (Fig. 7B, D). Thus, the BMP signaling pathway is being enhanced by the loss of *sec15* and this enhancement is completely blocked by RNAi knockdown of the BMP receptor *wit*.

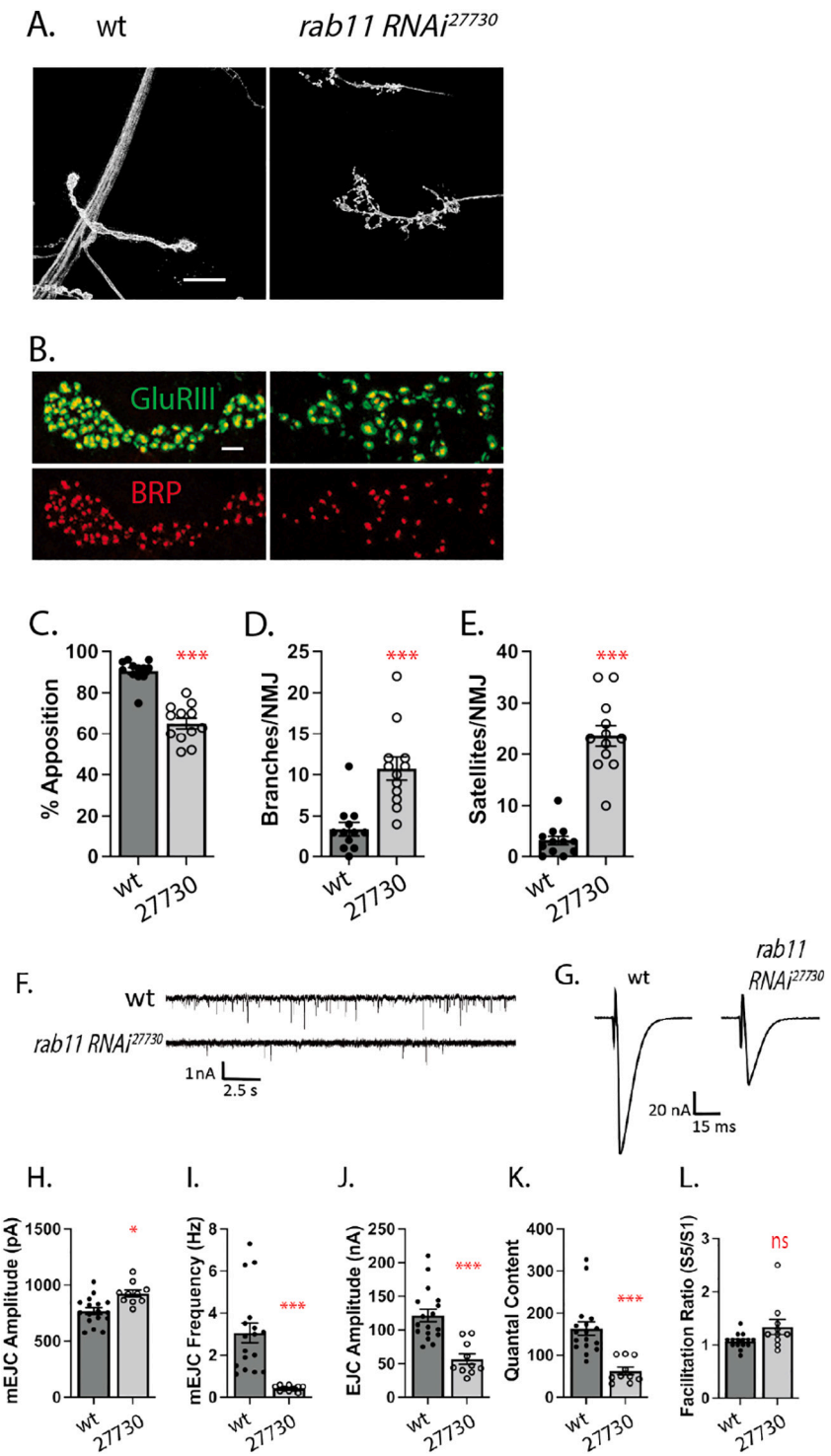

Fig. 6. Sec15 knockdown phenotype is mimicked by Rab11 knockdown. **A)** Confocal images of representative type 1b synaptic boutons of muscle 4 NMJs. Preparations are labeled with antibodies to HRP (blue), BRP (red), and GluRIII (green). Shown are representative NMJs from control larvae (*elav-Gal4, UAS-DCR2/+*), or a *UAS- rab11 RNAi* transgenic larvae (*elav-Gal4, UAS-DCR2/+; UAS-rab11 RNAi* ^{27730}*/+*). Scale bar is equal to 20 μm. **B)** Enlarged confocal image of the muscle 4 type 1b boutons of genotypes listed in A. Images are labeled with α-BRP (red) and α-GluRIII (green). Scale bar is equal to 2 μm. **C–E)** Bar graphs of % GluRIII clusters apposed by BRP punctum, number of axonal branches/NMJ, and the number of satellite boutons/NMJ for the wild type and *UAS-rab11 RNAi* ^{27730}. **F)** Representative recording of spontaneous excitatory currents in muscle 6 held at −70 mV for genotypes listed in (A) **G)** Representative recordings of stimulated currents elicited by a single suprathreshold electrical pulse for genotypes listed in (A). Figures show the average current waveform of 10 consecutive stimulations. **H–L)** Bar graphs showing various measures of synaptic physiology for the genotypes listed in (A), including **H)** mEJC amplitude**, I)** mEJC frequency **J)** EJC amplitude, **K)** number of synaptic vesicles released or quantal content, and **L)** the facilitation of synaptic currents by five successive high frequency stimulations or the facilitation ratio. Error Bars represent SEM. * denotes significant difference at the $p < 0.05$, ** $p < 0.01$, or *** $p < 0.001$ level using one-way ANOVA with Tukey's post-hoc test.

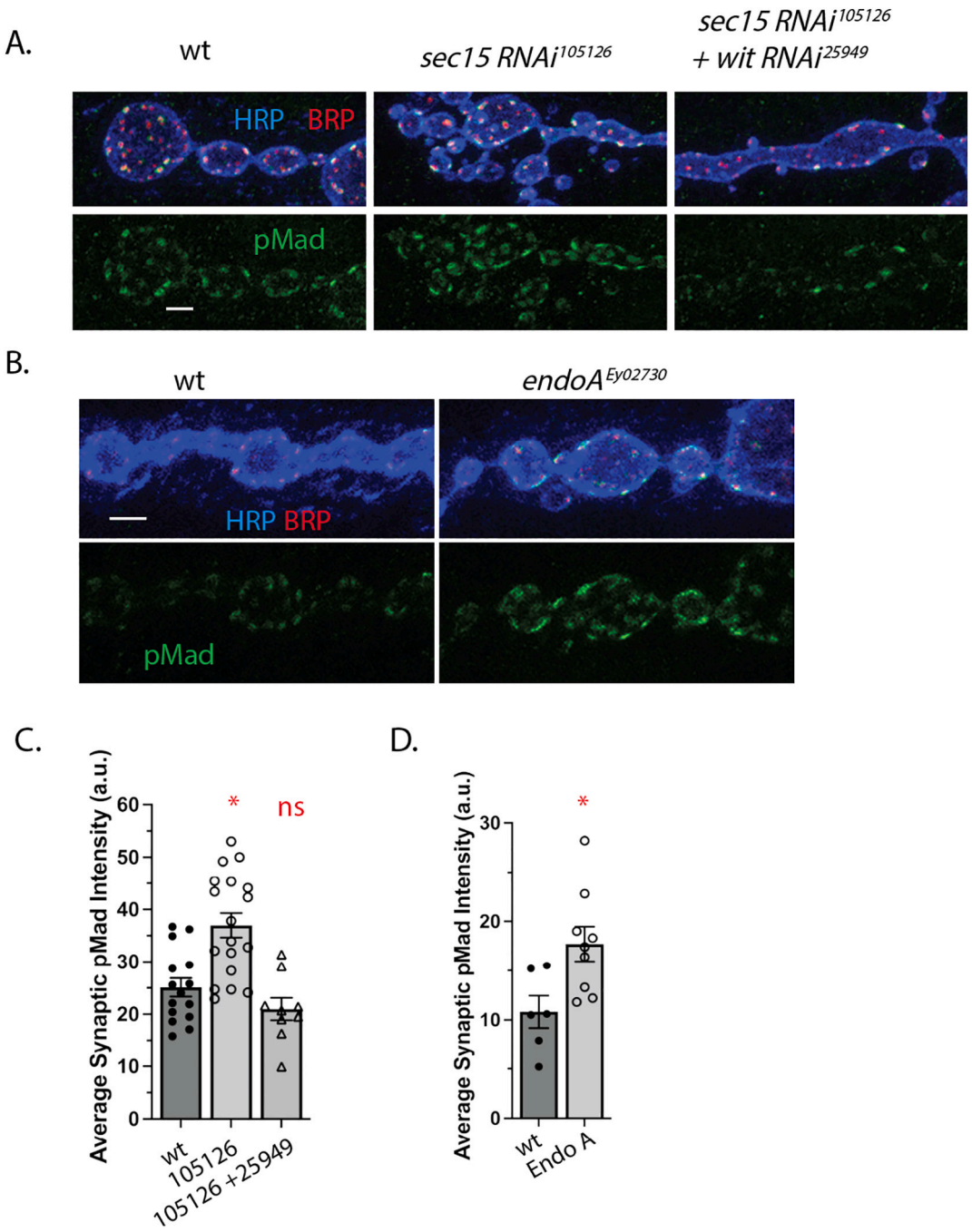

Fig. 7. Levels of the phosphorylated form of the BMP signaling protein Mad are increased in Sec15 knockdowns. **A)** Confocal images of the muscle 4 NMJs from wild type larvae (*elav-Gal4, UAS-DCR2/+*) or larvae expressing *UAS- sec15 RNAi* transgene (*elav-Gal4, UAS-DCR2/UAS-sec15 RNAi*^{105126}), or co-expressed *UAS-sec15 RNAi* and *UAS-wit RNAi* transgene (*elav-Gal4, UAS-DCR2/UAS-sec15 RNAi*^{105126}*; UAS-wit RNAi*^{25949}*/+*). Larvae are labeled with α-HRP (Blue), α-BRP (Red), and α-pMad (green). **B)** Confocal image of NMJ of muscle 4 of wild type larvae alone (+/+), or the *endophilinA* mutant larvae *endoA*^{EYO2730} (*endoA*^{EYO2730}*/endoA*^{EYO2730}) **C)** Bar graph of the average intensity of the synaptic pMad antibody signal for the genotypes listed in (A). * denotes significant difference at the $p < 0.05$ level using one-way ANOVA with Tukey's post-hoc test. **D)** Bar graph of the average intensity of the synaptic pMad antibody signal for the genotypes listed in B. * denotes significant difference at the $p < 0.05$ level using Student's *t*-test.

3.7. Interruption of BMP signaling attenuates many, but not all, morphological defects resulting from Sec15 knockdown

Since we have shown that the BMP signaling pathway is activated by the loss of Sec15 we wanted to determine which, if any, of the specific phenotypes seen after knockdown of Sec15 were attributable to increased BMP signaling. To do this, we first used the RNAi transgene directed against the BMP receptor Wit. Expression of *UAS-wit RNAi* alone had no significant effect on the morphology of the NMJ (Fig. 8). However, expression of UAS-*wit RNAi* simultaneously with *UAS-sec15 RNAi* caused a significant reduction in both the number of branches as well as the formation of satellite boutons normally seen when *UAS-sec15 RNAi* is expressed alone (Fig. 8C, D). This is an indication that these phenotypes result, at least in part, from a Sec15 KD-mediated enhancement of BMP signaling and not as a direct effect of the loss of Sec15. Interestingly not all of the morphological phenotypes were reduced. The percentage of GluR clusters apposed to BRP in *sec15 RNAi-wit RNAi* double knockdown animals was similar to animals expressing

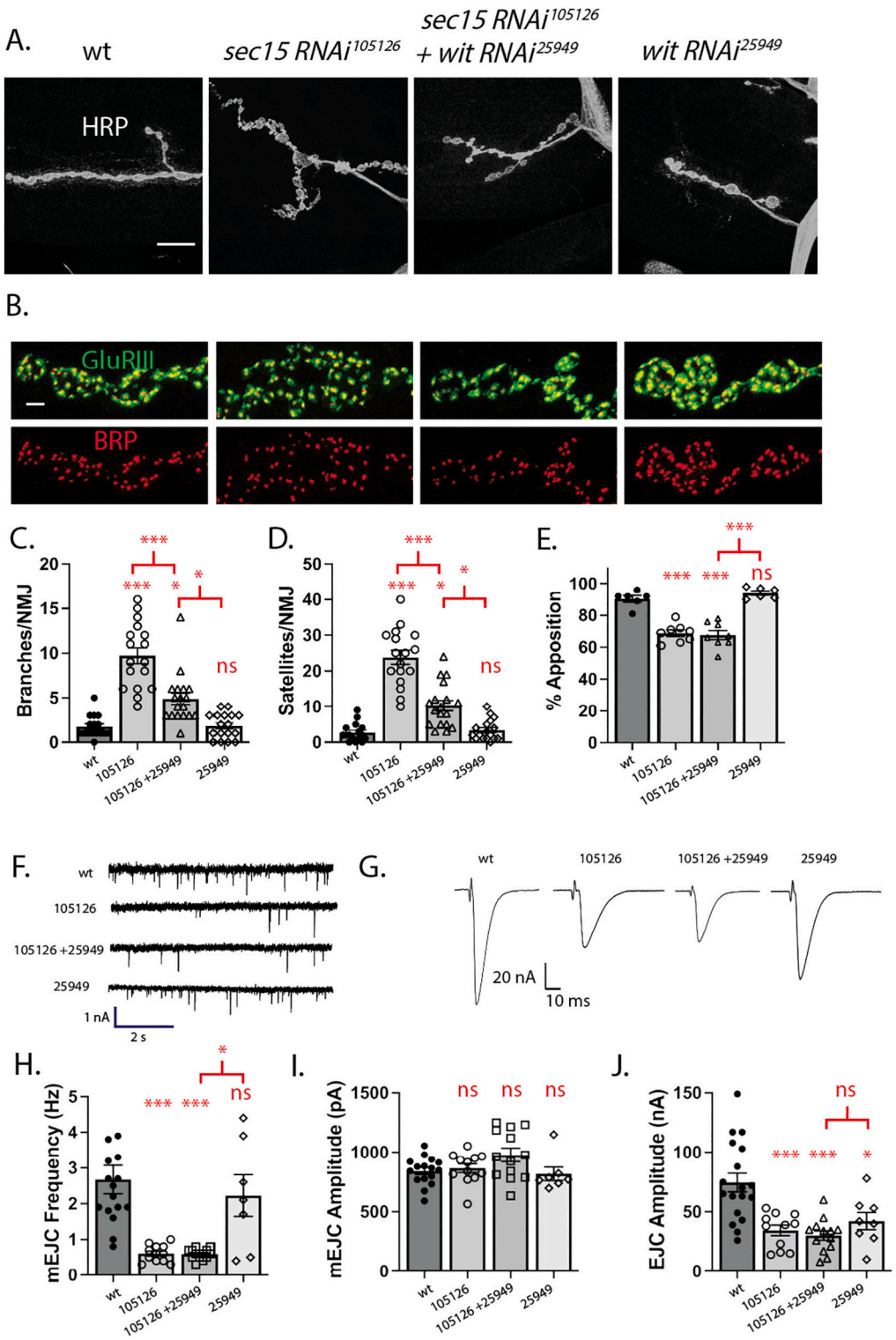

Fig. 8. Morphological defects seen in sec15 knockdowns are reduced by knockdown of the BMP receptor Wishful thinking. **A)** Confocal images of the NMJ of *Drosophila* 3rd instar larval muscle 4. Preparations are labeled with antibodies to HRP (white). Shown are representative NMJs from wild type larvae (*elav-Gal4, UAS-DCR2/+*) or with a *UAS- sec15 RNAi* transgene (*elav-Gal4, UAS-DCR2/UAS-sec15 RNAi*^{105126}), or both *UAS-sec15 RNAi* and *UAS-wit RNAi* (*elav-Gal4, UAS-DCR2/UAS-sec15 RNAi*^{105126}*; UAS-wit RNAi*^{25949}*/+*), or *UAS-wit RNAi* alone (*elav-Gal4, UAS-DCR2/+; UAS-wit RNAi*^{25949}*/+*). Scale bar is equal to 20 μm. **B)** Enlarged confocal image of muscle 4 type 1b boutons of the genotypes listed in (A), showing staining for BRP (red), and GluRIII (Green). Scale bar is equal to 2 μm. **C–E)** Quantitation of several morphological aspects of the NMJs for the genotypes listed in (A), including **C)** average branches per NMJ, **D)** average satellite boutons per NMJ, and **E)** percentage of glutamate receptor clusters apposed by BRP punctum. **F)** Representative mEJCs and **G)** EJC's for the listed genotypes. **H–J)** Quantitation of several electrophysiological properties for the genotypes listed. For all graphs * denotes significant difference at the $p < 0.05$, ** $p < 0.01$, or *** $p < 0.001$ level using one-way ANOVA with Tukey's post-hoc test.

UAS-sec15 RNAi alone (Fig. 8E). This result suggests two separable effects of Sec15 knockdown. The apposition phenotype is likely a direct effect of the loss of Sec15, while the branching and satellite bouton formation phenotypes are a result of the secondary effect of Sec15 KD, enhanced BMP signaling.

We next tested the effects of Wit KD on synaptic transmission in Sec15 KDs. Since the Wit KD did not affect the synaptic apposition defects we wondered whether it also would similarly not affect the synaptic physiology defects. A previously identified BMP-enhancing mutant, *daughters against decapentaplegic* (*dad,*) shows expanded and irregular NMJ morphology and yet exhibits no change in EJC size (Lee et al., 2016), suggesting that enhanced BMP signaling itself does not cause the synaptic physiological defects. We found that, similar to synaptic apposition, the frequency of mEJCs and the amplitude of EJCs in the Sec15 KD were both not rescued by a concurrent Wit KD, indicating these phenotypes, as we hypothesized, were independent of enhanced BMP activation and may result directly from the loss of Sec15. Expression of the *UAS-wit RNAi* by itself cause a reduction in EJC size (Fig. 8J) so it is unclear, in the case of the EJC, whether KD of Wit failed to rescue the EJC phenotype or whether it merely caused an additional reduction in EJC via a different mechanism induced by loss of the Wit receptor. The result from the mini frequency is clear, however, and suggests that the synaptic transmission defects are caused by loss of Sec15 and not a secondary effect caused by increased BMP signaling.

A possible problem that could arise when using multiple UAS constructs is titration of the Gal4 protein. We found, however, that expression of another UAS-RNAi targeting another member of the BMP receptor complex, saxophone (sax), concurrently with *sec15* RNAi was completely ineffective at reducing the branching and satellite phenotypes caused by Sec15 knockdown (Fig. S3). Thus, the reduction in *sec15* phenotypes seen with the concurrent expression of *wit* RNAi is not a result of titration of Gal4.

3.8. *Blocking BMP with a wit null mutant does not completely eliminate morphological phenotypes induced by knockdown of Sec15*

We have found that by blocking the BMP pathway with RNAi for the Wit receptor, we can completely eliminate the formation of pMad and

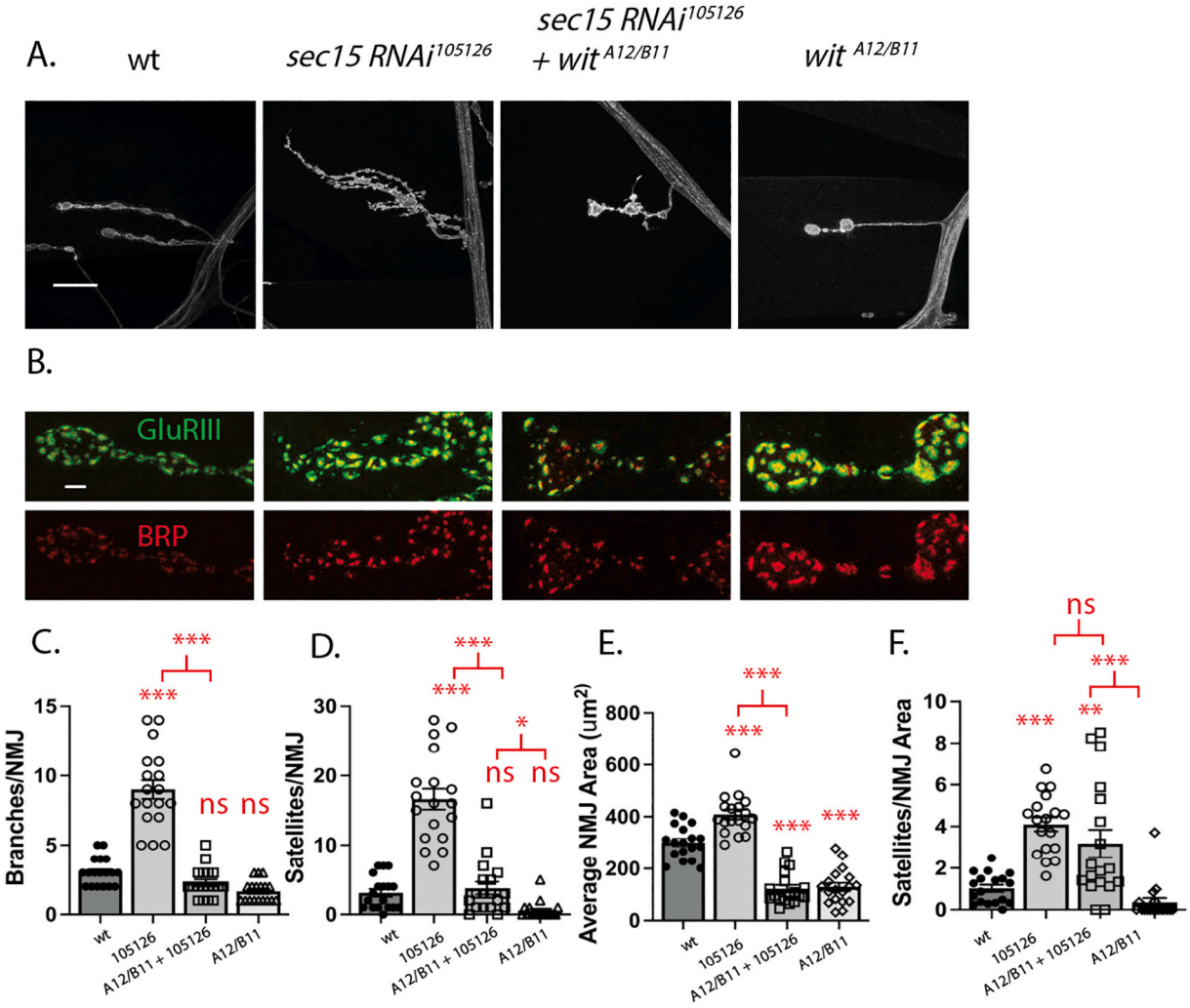

Fig. 9. Morphological defects seen in *sec15* knockdowns are reduced but not eliminated by BMP receptor *wishful thinking* mutant. **A)** Confocal images of the muscle 4 NMJs labeled with α-HRP (blue), α-BRP (red), and α-GluRIII (green) from wild type larvae (*elav-Gal4, UAS-DCR2/+*) or larvae expressing a *UAS- sec15 RNAi* transgenic larvae (*elav-Gal4, UAS-DCR2/UAS-sec15 RNAi*^{105126}), *UAS-sec15 RNAi* in a *wit* mutant background (*elav-Gal4, UAS-DCR2/UAS-sec15 RNAi (105126); wit*^{A12}*/wit*^{B11}), or *wit* mutant alone (*elav-Gal4, UAS-DCR2/+; wit*^{A12}*/wit*^{B11}). Scale bar is equal to 20 μm. **B)** Enlarged confocal image of synaptic boutons of muscle 4 of the genotypes listed in (A). Boutons are stained with α-GlurIII (Green) and α-BRP (Red). Scale bar is equal to 2 μm. **C–F)** Bar graphs of several morphological aspects of the NMJs in genotypes listed in (A), including **C)** average branches per NMJ, **D)** average satellite boutons per NMJ, E) average NMJ area, and F) number of satellite boutons per NMJ area. For all graphs * denotes significant difference at the $p < 0.05$, ** $p < 0.01$, or *** $p < 0.001$ level using one-way ANOVA with Tukey's post-hoc test.

partially reduce the branching and satellite bouton phenotypes seen after Sec15 knockdown. Although unlikely because of the complete loss of pMad enhancement, partial rescue of the branching and satellite bouton phenotypes may be due to an incomplete knockdown of Wit protein by the RNAi transgene. Therefore, we repeated these experiments using a *wit* null mutant background where all Wit protein is presumably absent (Marqués et al., 2002). We expressed the *UAS-sec15 RNAi* transgene in the $wit^{A12/B11}$ mutant background. In agreement with previous studies, we found that $wit^{A12/B11}$ mutant NMJs are dramatically reduced in size and the number of branches (Fig. 9A, C, D). When the *UAS-sec15 RNAi* was expressed in the *wit* mutant background the NMJs remained small with few branches and satellites, again an indication that these phenotypes may result from enhancement of BMP signaling (Fig. 9A, C, D, E). However, there was a significant increase in the number of satellites over what was seen in the *wit* mutant alone (Fig. 9D). Because of the substantial reduction in NMJ size in the wit mutant larvae (Fig. 9E), we quantified the changes in morphology after adjusting for the reduced size. When normalized for NMJ area, we found that the magnitude of the increase in satellite formation was similar to that seen for the *UAS-sec15 RNAi* expressed in the wild-type background (Fig. 9F). In conclusion, blocking the BMP signaling pathway is capable of reducing some but not all of the morphological effects resulting from the loss of presynaptic *sec15*. The fact that some effects persisted suggests that while some Sec15 knockdown defects may be caused by enhanced BMP signaling, satellite bouton formation in particular is at least partially independent of enhanced BMP signaling and may result directly from the loss of Sec15.

3.9. Sec 15 KD results in loss of extracellular vesicle release from neurons

During the course of our experiments with the Sec15 KD we noticed a lack of a punctate HRP staining that normally surrounds the presynaptic

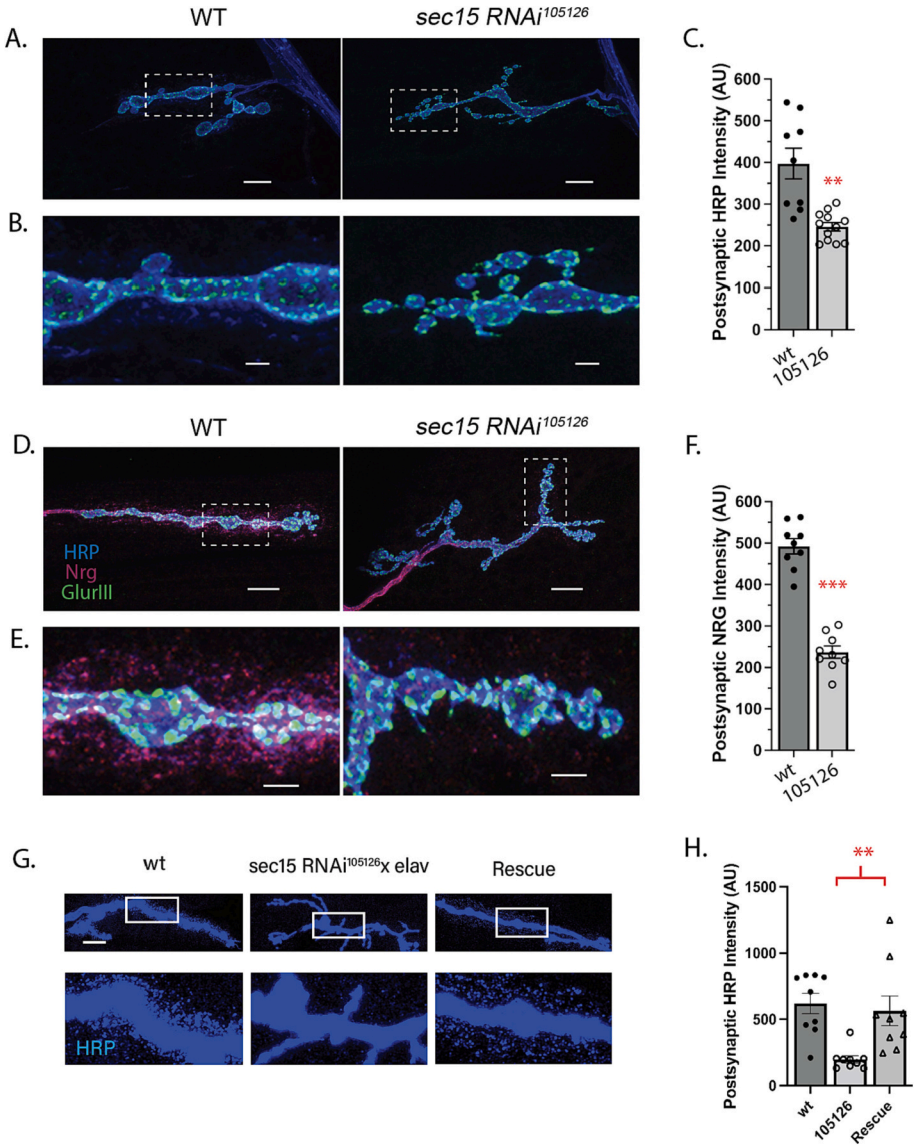

Fig. 10. Extracellular vesicle release is reduced in Sec15 KDs. **A)** Representative image of NMJs of wt and *sec15* RNAi larva. NMJs are stained with α-HRP and α-GluRIII (green). Scale bar represents 10 μm. **B)** Enlarged image of boxed portion of fig. A. Scale bar represents 2.5 μm. **C)** Quantitation of HRP staining in the area in proximity to the presynaptic neuron. **D)** Representative image of NMJs of wt and *sec15* RNAi larva. NMJs are stained with α-neuroglian (NRG, red) and α-GluRIII (green). Scale bar represents 10 μm **E)** Enlarged image of boxed portion of fig. D. Scale bar represents 2.5 μm. **F)** Quantitation of Neuroglian staining in the area in proximity to the presynaptic neuron. **G)** Representative HRP staining of control (left), UAS-$sec15^{105126}$ RNAi (middle) and UAS-$sec15^{105126}$ RNAi + UAS-sec15 -RNAi resistant (right, rescue). **H)** Quantification of postsynaptic HRP in the conditions listed for G. For all graphs * denotes significant difference at the ** $p < 0.01$, or *** $p < 0.001$ level using one-way ANOVA with Tukey's post-hoc test.

arbor. This punctate staining has been attributed to the release of extracellular vesicles from the presynaptic neuron (Korkut et al., 2013; Walsh et al., 2021). Staining for the presynaptically-derived protein Neuroglian (Nrg) has also been demonstrated to be a good measure of extracellular vesicle release (Walsh et al., 2021; Blanchette et al., 2022). We set out to quantify the lack of extracellular vesicle release by measuring the amount of HRP or Nrg staining in Sec15 knockdowns compared to control. We found that there was a highly significant decrease in the staining of both HRP and Nrg -positive extracellular vesicles in the area surrounding the presynaptic neuron in Sec15 KDs when compared to control (Fig. 10 A–D), indicating that Sec15 also plays a role in the release extracellular vesicles at this synapse. To demonstrate the specificity of our Sec15 KD we expressed our RNAi resistant *sec15* in order to rescue the RNAi induced extracellular vesicular phenotype. We found that the expression of Sec15 presynaptically was able to completely rescue the loss of extracellular vesicular release at these synapses (Fig. 10 G,H).

Rab11 RNAi caused a similar reduction in HRP and Neuroglian (Nrg) staining (Fig. S4) consistent with prior reports on the involvement of Rab11 in extravesicular release (Korkut et al., 2013; Walsh et al., 2021). Thus, Rab11, and Sec15 are also both involved in the formation and/or release of extracellular vesicles at this synapse.

4. Discussion

The exocyst protein complex has been shown to be necessary for secretion in yeast (Novick et al., 1980; Novick, 2014). In metazoan systems, the complex is not necessary for many types of vesicle fusion but rather seems to have evolved as a mechanism for targeting vesicles to specific sites for delivery of membrane lipids and proteins (Hsu et al., 2004; Emery and Knoblich, 2006; Heider and Munson, 2012; Picco et al., 2017). Here, we show that knockdown of Sec15 causes a number of important defects at the *Drosophila* NMJ including mislocalization of important synaptic proteins, defects in the spontaneous and stimulated release of synaptic vesicles, defects in the release of extracellular vesicles, and the inability to form an appropriate synaptic arbor at the NMJ. We also show *rab11* KD has almost identical phenotypes as the sec15 KD, suggesting the products of these two genes act in a molecular pathway that ensures proper development of both structure and function of the NMJ in *Drosophila*. Rab11 vesicles are primarily associated with recycling endosomes (Wandinger-Ness and Zerial, 2014) as well as release of extracellular vesicles (Korkut et al., 2013; Walsh et al., 2021), suggesting that the loss of either Rab11 or Sec15 specifically blocks 1) movement of vesicles progressing from the recycling endosome to the cell surface and 2) the mechanisms involved in the formation or release of extracellular vesicles.

4.1. Mechanism of exocyst at the NMJ

A role for the exocyst in Rab11-vesicle trafficking has been proposed to aid in the maintenance of epithelia cell polarity (Langevin et al., 2005; Guichard et al., 2010), recycling transferrin receptors (Takahashi et al., 2012), and maintenance of receptor tyrosine kinases at the leading edge of migrating *Drosophila* border cells (Assaker et al., 2010). In all cases, the recycling endosome is vital to maintaining proteins at a critical location on the cell surface. A similar mechanism may be at work in our study, with the recycling endosome being responsible for trafficking and precisely locating proteins and lipids on the surface of the neuron. In our study the levels of synaptic BRP are decreased and it is the loss of this protein, and perhaps other important synaptic proteins, that may lead to the observed physiological defects. As the movement of material from recycling endosome to the plasma membrane is subject to modulation (Khodosh et al., 2006; Ren and Guo, 2012; Welz et al., 2014), our results highlight an important potential mechanism for regulating the strength of neuronal synapses.

We have also demonstrated the loss of exocyst function in the NMJ causes an increase in BMP signaling as measured by an increase in pMad at the NMJ, likely through a mechanism in which activated BMP receptors are trapped in an activated state by their reduced movement through the endosomal trafficking pathway (Sadowski et al., 2009; Rodal et al., 2011; Deshpande and Rodal, 2015). The increased BMP signaling was completely blocked by Wit receptor knockdown. Even in this situation however, many of the phenotypic changes brought on by *sec15 RNAi* expression persisted, suggesting a more direct effect of the loss of Sec15. The persistence of *sec15 RNAi*-mediated morphological phenotypes were not likely due to an incomplete removal of the Wit receptor by RNAi as the morphologic phenotypes were seen in the *wit* null mutant as well. These results indicate that while enhanced BMP signaling, a secondary effect of the loss of the exocyst, does contribute to increased branching and satellite formation, the loss of the exocyst itself directly contributes as well. We propose that the augmentation of the satellite phenotype seen when BMP signaling is enhanced is likely a product of the combination of stimulated growth of the NMJ arbor and loss of the Sec15-mediated target specificity in vesicle fusion. The result is a more random non-stereotypical synaptic arbor. Conversely, the loss of BRP positive synapses and the functional synaptic defects seem to be completely independent of enhanced BMP signaling, suggesting a direct involvement of Sec15 in development or maintenance of BRP positive active zones. Another possibility could be that loss of Sec15 also enhances the wingless (Wg) or other cellular signaling pathways in a manner similar to the enhancement of BMP signaling. Enhancement of Wg signaling has been shown to cause the formation of satellite boutons (Franco, 2004), as well as altering the distribution of BRP positive active zones (Viquez et al., 2009). It is interesting that we do not appear to see any pathfinding defects as is seen in other neuronal preps (Vega and Hsu, 2001; Murthy et al., 2003; Mehta et al., 2005). It is likely that these events may occur at a developmental point prior to KD of Sec15 or conversely only the minimal Sec15 found after RNAi induced KD is sufficient for this task. This also highlights an inherent advantage of studying the exocyst with RNAi at the *Drosophila* NMJ, as pathfinding defects would prevent characterization of exocyst functions that are necessary at later time periods in development.

4.2. Loss of exocyst and Rab11 function results in defective synaptic physiology

In our study, using RNAi knockdown that targets Sec15 specifically in neurons, we found that loss of the exocyst can affect both spontaneous and evoked neurotransmission. Since the effects on synaptic transmission seen here were mimicked by Rab11 knockdown, the mechanism likely involves both the exocyst and Rab11. This phenotype was not fully rescued by our RNAi resistant overexpression of Sec15, casting some doubt on this result. We believe however, the reduction in EJC amplitude is a result of loss of the Sec15 protein based on the fact we see the phenotype in 3 separate *sec15* RNAi constructs as well as the *rab11* RNAi construct. It is unclear then, why many earlier studies do not see a similar reduction in synaptic transmission. One possibility is Sec15 may play different roles at other synapses such as the retinal synapse used in another *sec15* study (Mehta et al., 2005). A study that did use RNAi directed towards the exocyst subunit *sec10* at the *Drosophila* NMJ did not show an effect on EJC amplitude (Andrews et al., 2002). In this same study the *sec10* RNAi also did not show any effect on morphology of the synapse, perhaps pointing to a reduced efficacy of the RNAi in that study since we see a clear effect on morphology with our *sec10* RNAi. Other possibilities include differential effects of the various subunits on synaptic transmission. Koon et al. speculate that the null *exo70* mutant used in their study is not lethal because the exocyst is capable of functioning a reduced level without it and hence is on some level dispensable. It may turn out that some subunits of the exocyst are indispensable for all function while other subunits are critical only to certain functions of this protein complex or are more dispensable in general. Lastly, another possibility is the Ca^{2+} concentrations used in various studies. The lower

Ca^{2+} concentration used in our study may unmask defects that can be overcome at higher Ca^{2+} concentrations. We plan to further characterize the effect of Sec15 on synaptic vesicle dynamics and Ca^{2+} dependence of synaptic transmission in future studies.

How then do Sec15 and Rab11 affect the release of synaptic vesicles? Direct involvement of a Rab11-mediated event at later stages of the synaptic vesicle release process, such as docking and priming, would seem unlikely as these vesicles are primarily associated with Rab3, although the possibility cannot be ruled out. It is interesting that Rab11 KD has a much greater effect on synaptic transmission than elimination of Rab3 (Graf et al., 2009). Rab11 is also associated with synaptic vesicles and has been implicated in some forms of synaptic vesicle recycling (Pavlos and Jahn, 2011; Inoshita et al., 2017; Kokotos et al., 2018). Rather than acting directly in the release of synaptic vesicles, Sec15 and Rab11 may affect synaptic vesicle release secondarily through mechanisms that control trafficking and availability of synaptic vesicles. One possibility is an effect on the recycling of synaptic vesicles that necessitate movement through endosomal compartments. In this case either one of the steps involved in recycling of the synaptic vesicle requires Rab11 and Sec15 or alternatively the loss of the later recycling steps in turn effects earlier upstream trafficking events in other endosomal compartments.

Another alternative that could potentially explain the decreased synaptic transmission would be a loss of proteins or lipids normally provided to the AZ by the recycling endosome or extracellular vesicles. These factors are critical for the development or maintenance of the release site itself, and loss would perhaps be analogous to the loss of basolateral *E*-Cadherin in epithelial cells after the loss of exocyst function (Langevin et al., 2005). In support of this role, we saw a reduction in the levels of BRP in some AZs. The loss of BRP containing AZs likely contributes to the reduced synaptic strength, as loss of BRP is known to decrease synaptic transmission (Kittel et al., 2006; Peled and Isacoff, 2011). However, Sec15 or Rab11 knockdown each led to a much greater reduction in evoked vesicle release than would be expected by the functional loss of these AZs we see here as the complete loss of BRP causes a 70 % decrease in EJC amplitude and no change in spontaneous frequency (Kittel et al., 2006) while we see a ~50 % decrease with a relatively modest change in BRP concentrations. Future experiments will be necessary to determine the mechanism underlying the role of the exocyst in synaptic function and may lead to fundamental changes in our understanding of the organization and movement of vesicles at synapses.

4.3. Extracellular vesicle release

Extracellular vesicles (exosomes and micro-vesicles) have been shown to be an important mechanism for trans-synaptic signaling. An interesting result we report here is that presynaptic KD of either Sec15 or Rab11 causes a reduction in extracellular vesicles (EVs) in the post-synaptic region. The ability of Rab11 to effect EV signaling has been reported previously (Korkut et al., 2013; Walsh et al., 2021) but here we extend that to include Sec15. Relatively little is known about the precise mechanisms of release of EVs but likely it involves the targeting and fusion of multi-vesicular bodies (MVBs) to the cell membrane with subsequent release of the vesicles that are contained within (van Niel et al., 2018). Future work will be necessary to characterize the specific type of vesicle involved in the Sec15 signaling as well as the specific cargoes and exocyst subunits utilized in the process.

5. Conclusions

Our study uncovered a function of the exocyst in motor neurons where it promotes the formation of the synaptic arbor as well as promoting proper synaptic connections. Our results indicate that loss of Sec15-mediated exocytosis results in a wide array of defects in the synapse, pointing to a number of aspects of synapse development and maintenance, both direct and indirect, that are mediated by *sec15*. We propose a model in which Sec15, in conjunction with Rab11, aids in movement of material through the recycling endosome to the plasma membrane of the neuron as well as allowing for release of extracellular vesicles and proper extracellular vesicle signaling with the postsynaptic cell.

Rab11 has been shown to be involved in the accumulation of the Alzheimer's Aβ peptide (Li et al., 2012), and it has been genetically linked with late-onset Alzheimer's (Udayar et al., 2013). Rab11 has also been shown to interact with the Huntingtin gene and disruption of the normal function of *rab11* seems to be important in disease progression (Li et al., 2010). In *Drosophila*, expression of pathogenic Huntingtin protein disrupted endosomal trafficking and increased BMP signaling (Akbergenova and Littleton, 2017) and overexpression of Rab11 was capable of overcoming the synaptic defects found in this Huntington's disease model (Steinert et al., 2012). In addition, Rab11 has been shown to be important for the trafficking of amyloid precursor protein in Hela and N2a cells as well as the Drosophila NMJ (Rajendran et al., 2006; Walsh et al., 2021) Thus, the proposed targeted release pathway mediated by Rab11 and the exocyst likely plays an important role in mammalian synapse function as well as in the progression of disorders such as Alzheimer's and Huntington's diseases. Additionally, our findings point to a potentially important mechanism for mediating synaptic plasticity through regulation of vesicle trafficking and fusion by the recycling endosome.

CRediT authorship contribution statement

Chris J. Kang: Formal analysis, Investigation, Methodology. **Luis E. Guzmán-Clavel:** Formal analysis, Investigation, Methodology. **Katherine Lei:** Formal analysis, Investigation. **Martin Koo:** Formal analysis, Investigation. **Steven To:** Formal analysis, Investigation. **John P. Roche:** Conceptualization, Data curation, Formal analysis, Investigation, Methodology, Project administration, Supervision, Writing – original draft, Writing – review & editing.

Declaration of competing interest

The authors declare no competing interest.

Data availability

Data will be made available on request.

Acknowledgements

We thank Drs. Josef Trapani, Mona Wu-Orr and Avital Rodal for experimental assistance and helpful advice. We thank Avital Rodal for careful reading of the manuscript. We thank Dr. Nicholas Horton for helpful advice on the statistics. We thank Maureen Manning, Lori Nichols and Siri Palreddy for technical assistance. We thank Ethan Graf for Rab3 fly stocks and Aron DiAntonio for the GlurIII antibody. We thank Lampros Panagis and the Amherst Biological imaging center for help with the microscopy. We also thank the Bloomington and Vienna Stock Centers for fly strains and the Developmental Studies Hybridoma Bank for antibodies. This work was supported by Faculty Research Funds from Amherst College (J.P.R.) and NSF MRI award #2117798 awarded to Amherst College.

Appendix A. Supplementary data

Supplementary data to this article can be found online at https://doi.org/10.1016/j.mcn.2023.103914.

References

Akbergenova, Y., Littleton, J.T., 2017. Pathogenic Huntington alters BMP signaling and synaptic growth through local disruptions of endosomal compartments. J. Neurosci. 37, 3425–3439.

Andrews, H.K., Zhang, Y.Q., Trotta, N., Broadie, K., 2002. Drosophila sec10 is required for hormone secretion but not general exocytosis or neurotransmission. Traffic 3, 906–921.

Assaker, G., Ramel, D., Wculek, S.K., González-Gaitán, M., Emery, G., 2010. Spatial restriction of receptor tyrosine kinase activity through a polarized endocytic cycle controls border cell migration. Proc. Natl. Acad. Sci. 107, 22558–22563.

Bellen, H.J., 2004. The BDGP gene disruption project: single transposon insertions associated with 40% of Drosophila genes. Genetics 167, 761–781.

Blanchette, C.R., Scalera, A.L., Harris, K.P., Zhao, Z., Dresselhaus, E.C., Koles, K., Yeh, A., Apiki, J.K., Stewart, B.A., Rodal, A.A., 2022. Local regulation of extracellular vesicle traffic by the synaptic endocytic machinery. J. Cell Biol. 221, e202112094.

Boyd, C., 2004. Vesicles carry most exocyst subunits to exocytic sites marked by the remaining two subunits, Sec3p and Exo70p. J. Cell Biol. 167, 889–901.

Cai, H., Reinisch, K., Ferro-Novick, S., 2007. Coats, tethers, Rabs, and SNAREs work together to mediate the intracellular destination of a transport vesicle. Dev. Cell 12, 671–682.

Collins, C.A., DiAntonio, A., 2007. Synaptic development: insights from Drosophila. Curr. Opin. Neurobiol. 17, 35–42.

Echeverri, C.J., et al., 2006. Minimizing the risk of reporting false positives in large-scale RNAi screens. Nat. Methods 3, 777–779. https://www.nature.com/articles/nmeth1006-777.

Deshpande, M., Rodal, A.A., 2015. The crossroads of synaptic growth signaling, membrane traffic, and neurological disease: insights from *Drosophila*: synaptic signaling and membrane traffic in *Drosophila*. Traffic 17, 87–101.

Dickman, D.K., Lu, Z., Meinertzhagen, I.A., Schwarz, T.L., 2006. Altered synaptic development and active zone spacing in endocytosis mutants. Curr. Biol. 16, 591–598.

Dietzl, G., Chen, D., Schnorrer, F., Su, K.-C., Barinova, Y., Fellner, M., Gasser, B., Kinsey, K., Oppel, S., Scheiblauer, S., Couto, A., Marra, V., Keleman, K., Dickson, B. J., 2007. A genome-wide transgenic RNAi library for conditional gene inactivation in Drosophila. Nature 448, 151–156.

Dupraz, S., Grassi, D., Bernis, M.E., Sosa, L., Bisbal, M., Gastaldi, L., Jausoro, I., Caceres, A., Pfenninger, K.H., Quiroga, S., 2009. The TC10-Exo70 complex is essential for membrane expansion and axonal specification in developing neurons. J. Neurosci. 29, 13292–13301.

Emery, G., Knoblich, J.A., 2006. Endosome dynamics during development. Curr. Opin. Cell Biol. 18, 407–415.

Franco, B., 2004. Shaggy, the homolog of glycogen synthase kinase 3, controls neuromuscular junction growth in Drosophila. J. Neurosci. 24, 6573–6577.

Graf, E.R., Daniels, R.W., Burgess, R.W., Schwarz, T.L., DiAntonio, A., 2009. Rab3 dynamically controls protein composition at active zones. Neuron 64, 663–677.

Graf, E.R., Valakh, V., Wright, C.M., Wu, C., Liu, Z., Zhang, Y.Q., DiAntonio, A., 2012. RIM promotes calcium channel accumulation at active zones of the Drosophila neuromuscular junction. J. Neurosci. 32, 16586–16596.

Guichard, A., McGillivray, S.M., Cruz-Moreno, B., van Sorge, N.M., Nizet, V., Bier, E., 2010. Anthrax toxins cooperatively inhibit endocytic recycling by the Rab11/Sec15 exocyst. Nature 467, 854–858.

Guo, W., Roth, D., Walch-Solimena, C., Novick, P., 1999. The exocyst is an effector for Sec4p, targeting secretory vesicles to sites of exocytosis. EMBO J. 18, 1071–1080.

Hazuka, C.D., Foletti, D.L., Hsu, S-C, Kee, Y., Hopf, W., Scheller, R.H., 1999. The sec6/8 complex is located at neurite outgrowth and axonal synapse assebly domains. J. Neurosci. 19 (4), 1324–1334.

Heider, M.R., Munson, M., 2012. Exorcising the exocyst complex: exorcising the exocyst complex. Traffic 13, 898–907.

Hsu, S.-C., TerBush, D., Abraham, M., Guo, W., 2004. The exocyst complex in polarized exocytosis. Int. Rev. Cytol. 233, 243–265.

Inoshita, T., Arano, T., Hosaka, Y., Meng, H., Umezaki, Y., Kosugi, S., Morimoto, T., Koike, M., Chang, H.-Y., Imai, Y., Hattori, N., 2017. Vps35 in cooperation with LRRK2 regulates synaptic vesicle endocytosis through the endosomal pathway in Drosophila. Hum. Mol. Genet. 26, 2933–2948.

Keshishian, H., Kim, Y.-S., 2004. Orchestrating development and function: retrograde BMP signaling in the Drosophila nervous system. Trends Neurosci. 27, 143–147.

Khodosh, R., Augsburger, A., Schwarz, T.L., Garrity, P.A., 2006. Bchs, a BEACH domain protein, antagonizes Rab11 in synapse morphogenesis and other developmental events. Development 133, 4655–4665.

Kittel, R.J., Wichmann, C., Rasse, T.M., Fouquet, W., Schmidt, M., Schmid, A., Wagh, D. A., Pawlu, C., Kellner, R.R., Willig, K.I., et al., 2006. Bruchpilot promotes active zone assembly, Ca2+ channel clustering, and vesicle release. Science 312, 1051–1054.

Koh, T.-W., Verstreken, P., Bellen, H.J., 2004. Dap160/intersectin acts as a stabilizing scaffold required for synaptic development and vesicle endocytosis. Neuron 43, 193–205.

Kokotos, A.C., Peltier, J., Davenport, E.C., Trost, M., Cousin, M.A., 2018. Activity-dependent bulk endocytosis proteome reveals a key presynaptic role for the monomeric GTPase Rab11. Proc. Natl. Acad. Sci. U. S. A. 115, E10177–E10186.

Koon, A.C., Chen, Z.S., Peng, S., Fung, J.M.S., Zhang, X., Lembke, K.M., Chow, H.K., Frank, C.A., Jiang, L., Lau, K.-F., Chan, H.Y.E., 2018. Drosophila Exo70 is essential for neurite extension and survival under thermal stress. J. Neurosci. 38, 8071–8086.

Korkut, C., Li, Y., Koles, K., Brewer, C., Ashley, J., Yoshihara, M., Budnik, V., 2013. Regulation of postsynaptic retrograde signaling by presynaptic exosome release. Neuron 77, 1039–1046.

Langevin, J., Morgan, M.J., Rossé, C., Racine, V., Sibarita, J.-B., Aresta, S., Murthy, M., Schwarz, T., Camonis, J., Bellaïche, Y., 2005. Drosophila exocyst components Sec5, Sec6, and Sec15 regulate DE-cadherin trafficking from recycling endosomes to the plasma membrane. Dev. Cell 9, 365–376.

Lee, S.-H., Kim, Y.-J., Choi, S.-Y., 2016. BMP signaling modulates the probability of neurotransmitter release and readily releasable pools in Drosophila neuromuscular junction synapses. Biochem. Biophys. Res. Commun. 479, 440–446.

Li, J., Kanekiyo, T., Shinohara, M., Zhang, Y., LaDu, M.J., Xu, H., Bu, G., 2012. Differential regulation of amyloid-β endocytic trafficking and lysosomal degradation by apolipoprotein E isoforms. J. Biol. Chem. 287, 44593–44601.

Li, X., Valencia, A., Sapp, E., Masso, N., Alexander, J., Reeves, P., Kegel, K.B., Aronin, N., DiFiglia, M., 2010. Aberrant Rab11-dependent trafficking of the neuronal glutamate transporter EAAC1 causes oxidative stress and cell death in Huntington's disease. J. Neurosci. 30, 4552–4561.

Liebl, F.L., Chen, K., Karr, J., Sheng, Q., Featherstone, D.E., 2005. Increased synaptic microtubules and altered synapse development in Drosophila sec8 mutants. BMC Biol. 3, 1.

Liu, Z., Huang, Y., Hu, W., Huang, S., Wang, Q., Han, J., Zhang, Y.Q., 2014. dAcsl, the Drosophila ortholog of acyl-CoA synthetase long-chain family member 3 and 4, inhibits synapse growth by attenuating bone morphogenetic protein signaling via endocytic recycling. J. Neurosci. 34, 2785–2796.

Marie, B., Sweeney, S.T., Poskanzer, K.E., Roos, J., Kelly, R.B., Davis, G.W., 2004. Dap160/intersectin scaffolds the periactive zone to achieve high-fidelity endocytosis and normal synaptic growth. Neuron 43, 207–219.

Marqués, G., Bao, H., Haerry, T.E., Shimell, M.J., Duchek, P., Zhang, B., O'Connor, M.B., 2002. The Drosophila BMP type II receptor wishful thinking regulates neuromuscular synapse morphology and function. Neuron 33, 529–543.

Marrus, S.B., 2004. Differential localization of glutamate receptor subunits at the Drosophila neuromuscular junction. J. Neurosci. 24, 1406–1415.

McCabe, B.D., Marqués, G., Haghighi, A.P., Fetter, R.D., Crotty, M.L., Haerry, T.E., Goodman, C.S., O'Connor, M.B., 2003. The BMP homolog Gbb provides a retrograde signal that regulates synaptic growth at the Drosophila neuromuscular junction. Neuron 39, 241–254.

Mehta, S.Q., Hiesinger, P.R., Beronja, S., Zhai, R.G., Schulze, K.L., Verstreken, P., Cao, Y., Zhou, Y., Tepass, U., Crair, M.C., Bellen, H.J., 2005. Mutations in Drosophila sec15 reveal a function in neuronal targeting for a subset of exocyst components. Neuron 46, 219–232.

Murthy, M., Garza, D., Scheller, R.H., Schwarz, T.L., 2003. Mutations in the exocyst component Sec5 disrupt neuronal membrane traffic, but neurotransmitter release persists. Neuron 37, 433–447.

Novick, P., Field, C., Schekman, R., 1980. Identification of 23 complementation groups required for post-translational events in the yeast secretory pathway. Cell 21, 205–215.

Novick, P.J., 2014. A pathway of a hundred genes starts with a single mutant: isolation of sec1-1. Proc. Natl. Acad. Sci. 111, 9019–9020.

O'Connor-Giles, K.M., Ganetzky, B., 2008. Satellite signaling at synapses. Fly (Austin) 2, 259–261.

O'Connor-Giles, K.M., Ho, L.L., Ganetzky, B., 2008. Nervous wreck interacts with thickveins and the endocytic machinery to attenuate retrograde BMP signaling during synaptic growth. Neuron 58, 507–518.

Pavlos, N.J., Jahn, R., 2011. Distinct yet overlapping roles of Rab GTPases on synaptic vesicles. Small GTPases 2, 77–81.

Peled, E.S., Isacoff, E.Y., 2011. Optical quantal analysis of synaptic transmission in wild-type and rab3-mutant Drosophila motor axons. Nat. Neurosci. 14, 519–526.

Persson, U., Izumi, H., Souchelnytskyi, S., Itoh, S., Grimsby, S., Engström, U., Heldin, C.-H., Funa, K., ten Dijke, P., 1998. The L45 loop in type I receptors for TGF-β family members is a critical determinant in specifying Smad isoform activation. FEBS Lett. 434, 83–87.

Picco, A., Irastorza-Azcarate, I., Specht, T., Böke, D., Pazos, I., Rivier-Cordey, A.-S., Devos, D.P., Kaksonen, M., Gallego, O., 2017. The in vivo architecture of the exocyst provides structural basis for exocytosis. Cell 168, 400–412.e18.

Rajendran, L., Honsho, M., Zahn, T.R., Keller, P., Geiger, K.D., Verkade, P., Simons, K., 2006. Alzheimer's disease beta-amyloid peptides are released in association with exosomes. Proc. Natl. Acad. Sci. U. S. A. 103, 11172–11177.

Regehr, W.G., 2012. Short-term presynaptic plasticity. Cold Spring Harb. Perspect. Biol. 4, a005702.

Ren, J., Guo, W., 2012. ERK1/2 regulate exocytosis through direct phosphorylation of the exocyst component Exo70. Dev. Cell 22, 967–978.

Rodal, A.A., Motola-Barnes, R.N., Littleton, J.T., 2008. Nervous wreck and Cdc42 cooperate to regulate endocytic actin assembly during synaptic growth. J. Neurosci. 28, 8316–8325.

Rodal, A.A., Blunk, A.D., Akbergenova, Y., Jorquera, R.A., Buhl, L.K., Littleton, J.T., 2011. A presynaptic endosomal trafficking pathway controls synaptic growth signaling. J. Cell Biol. 193, 201–217.

Sadowski, L., Pilecka, I., Miaczynska, M., 2009. Signaling from endosomes: location makes a difference. Exp. Cell Res. 315, 1601–1609.

Salminen, A., Novick, P.J., 1989. The Sec15 protein responds to the function of the GTP binding protein, Sec4, to control vesicular traffic in yeast. J. Cell Biol. 109, 1023–1036.

Schindelin, J., Arganda-Carreras, I., Frise, E., Kaynig, V., Longair, M., Pietzsch, T., Preibisch, S., Rueden, C., Saalfeld, S., Schmid, B., Tinevez, J.-Y., White, D.J., Hartenstein, V., Eliceiri, K., Tomancak, P., Cardona, A., 2012. Fiji - an open source platform for biological image analysis. Nat. Methods 9. https://doi.org/10.1038/nmeth.2019.

Sigoillot, F.D., King, R.W., 2011. Vigilance and validation: keys to success in RNAi screening. ACS Chem. Biol. 6, 47–60.

Steinert, J.R., Campesan, S., Richards, P., Kyriacou, C.P., Forsythe, I.D., Giorgini, F., 2012. Rab11 rescues synaptic dysfunction and behavioural deficits in a Drosophila model of Huntington's disease. Hum. Mol. Genet. 21, 2912–2922.
Sweeney, S.T., Davis, G.W., 2002. Unrestricted synaptic growth in spinster—a late endosomal protein implicated in TGF-β-mediated synaptic growth regulation. Neuron 36, 403–416.
Takahashi, S., Kubo, K., Waguri, S., Yabashi, A., Shin, H.-W., Katoh, Y., Nakayama, K., 2012. Rab11 regulates exocytosis of recycling vesicles at the plasma membrane. J. Cell Sci. 125, 4049–4057.
TerBush, D.R., Maurice, T., Roth, D., Novick, P., 1996. The exocyst is a multiprotein complex required for exocytosis in Saccharomyces cerevisiae. EMBO J. 15, 6483.
Torroja, L., Packard, M., Gorczyca, M., White, K., Budnik, V., 1999. The Drosophila β-amyloid precursor protein homolog promotes synapse differentiation at the neuromuscular junction. J. Neurosci. 19, 7793–7803.
Udayar, V., Buggia-Prévot, V., Guerreiro, R.L., Siegel, G., Rambabu, N., Soohoo, A.L., Ponnusamy, M., Siegenthaler, B., Bali, J., Simons, M., Ries, J., Puthenveedu, M.A., Hardy, J., Thinakaran, G., Rajendran, L., 2013. A paired RNAi and RabGAP overexpression screen identifies Rab11 as a regulator of β-amyloid production. Cell Rep. 5, 1536–1551.
van Niel, G., D'Angelo, G., Raposo, G., 2018. Shedding light on the cell biology of extracellular vesicles. Nat. Rev. Mol. Cell Biol. 19, 213–228.
Vega, I.E., Hsu, S.-C., 2001. The exocyst complex associates with microtubules to mediate vesicle targeting and neurite outgrowth. J. Neurosci. 21, 3839–3848.
Viquez, N.M., Fuger, P., Valakh, V., Daniels, R.W., Rasse, T.M., DiAntonio, A., 2009. PP2A and GSK-3 act antagonistically to regulate active zone development. J. Neurosci. 29, 11484–11494.
Walsh, R.B., Dresselhaus, E.C., Becalska, A.N., Zunitch, M.J., Blanchette, C.R., Scalera, A. L., Lemos, T., Lee, S.M., Apiki, J., Wang, S., Isaac, B., Yeh, A., Koles, K., Rodal, A.A., 2021. Opposing functions for retromer and Rab11 in extracellular vesicle traffic at presynaptic terminals. J. Cell Biol. 220, e202012034 https://doi.org/10.1083/jcb.202012034.
Wandinger-Ness, A., Zerial, M., 2014. Rab proteins and the compartmentalization of the endosomal system. Cold Spring Harb. Perspect. Biol. 6, a022616.
Welz, T., Wellbourne-Wood, J., Kerkhoff, E., 2014. Orchestration of cell surface proteins by Rab11. Trends Cell Biol. 24, 407–415.
Wu, B., Guo, W., 2015. The exocyst at a glance. J. Cell Sci. 128, 2957–2964.
Wu, S., Mehta, S.Q., Pichaud, F., Bellen, H.J., Quiocho, F.A., 2005. Sec15 interacts with Rab11 via a novel domain and affects Rab11 localization in vivo. Nat. Struct. Mol. Biol. 12, 879–885.
Yao, K.-M., White, K., 1994. Neural specificity of elav expression: defining a Drosophila promoter for directing expression to the nervous system. J. Neurochem. 63, 41–51.
Zhang, X.-M., Ellis, S., Sriratana, A., Mitchell, C.A., Rowe, T., 2004. Sec15 is an effector for the Rab11 GTPase in mammalian cells. J. Biol. Chem. 279, 43027–43034.
Zito, K., Parnas, D., Fetter, R.D., Isacoff, E.Y., Goodman, C.S., 1999. Watching a synapse grow: noninvasive confocal imaging of synaptic growth in Drosophila. Neuron 22, 719–729.